

Lunar Accretion from an Impact-Generated Disk

E. Kokubo

National Astronomical Observatory

R. M. Canup

Southwest Research Institute

S. Ida

Tokyo Institute of Technology

We review current models for the accumulation of the Moon from an impact-generated debris disk. Such a disk is dynamically distinguished by its substantial mass relative to the Earth and a very centrally condensed radial profile, with a mean orbital radius near the classical Roche limit. In the inner protolunar disk, accretion is inhibited by tidal forces. Typically, a single large moon accretes just outside the Roche limit, at a distance of about $3.5\text{--}4.0 \times$ the Earth's radius. A simple relationship between the fraction of the disk mass that is incorporated into the final moon and the initial disk angular momentum has been determined from simulations spanning a wide range of initial conditions, collisional parameterizations, and numerical resolutions. Predicted accretion yields range from 10% to 55%, with most of the remaining material scattered onto the Earth. Recent N-body simulations show the formation of transient gravitational instabilities in the inner disk, leading to rapid disk-spreading rates. These results may, however, be affected by current models' neglect of the thermal state of the disk material. Analyses of the orbital evolution of material due to tidal interaction with the Earth suggest that remnants of the initial accretion phase will likely be accumulated by either the largest moon or the Earth, leaving a single moon in most cases.

1. INTRODUCTION

Hydrodynamic simulations of potential lunar-forming impacts (*Kipp and Melosh*, 1986, 1987; *Benz et al.*, 1986, 1987, 1989; *Cameron and Benz*, 1991; *Cameron*, 1997; *Cameron and Canup*, 1998; see also chapter by *Cameron*, 2000) demonstrate the plausibility of the basic impact hypothesis. These simulations predict the ejection of roughly a lunar-mass worth of material into orbit following an off-center impact by an object with a mass close to that of Mars. The resulting debris cloud is centrally condensed, with a mean orbital radius of $2\text{--}3 R_{\oplus}$, or at about the Roche limit for silicate density materials ($a_R = 2.9 R_{\oplus}$), where R_{\oplus} is the radius of the Earth. The predicted initial state of material ejected into this protolunar cloud is dependent on the simulation specifics, with temperatures ranging from those of a vaporous cloud to those of a mixture of solid and molten material.

Initial modeling of the evolution of an impact-generated disk focused on how such a disk might viscously spread and become subject to collapse due to gravitational instability (*Ward and Cameron*, 1977, hereafter *WC77*; *Thompson and Stevenson*, 1988). Another question was why a disk of material roughly centered on the Roche limit should yield a single large moon, while similarly located systems around the outer planets consisted of rings and multiple small satellites. The first model of lunar accumulation from an impact-generated protolunar disk utilized a statistical model

of accretion that included tidal inhibition of accretion in the region surrounding the Roche limit (*Canup and Esposito*, 1996). Canup and Esposito found that systems of multiple small moons appeared to be probable outcomes. They suggested that the easiest way to form the Moon was to begin with a lunar-mass of material exterior to a_R , where a_R is the Roche limit radius, and that the most favorable impacts appeared to be those with about twice the angular momentum of the Earth-Moon system.

Accretion simulations utilizing direct N-body orbit integrations with $\sim 10^3$ initial ~ 100 -km-sized bodies (*Ida et al.*, 1997, hereafter *ICS97*) revealed disk-wide scattering among the moonlets. These interactions cleared the inner protolunar disk, leaving a single large moon at $3\text{--}4 R_{\oplus}$ in two-thirds of cases, and two large moons in one-third of cases. Scattering onto the Earth resulted in significant mass loss from the disk and net accretion yields below 50%. Thus an initial disk mass of at least $2 M_{\zeta}$ (where M_{ζ} is lunar mass) appeared required to yield a lunar-sized moon.

Recently, *Kokubo et al.* (2000, hereafter *KIM00*) have performed similar simulations using $N = 10,000$ particles. While the accretion yields found by *KIM00* are similar to those in *ICS97*, the *KIM00* simulations resolve the development of spatial structure in the disk that was only vaguely observable in the *ICS97* runs. This structure is found to be the dominant mechanism for angular momentum and mass transfer in the N-body simulations. About 10% of the *KIM00* runs produced two large moons outside the Roche limit.

Modeling of the tidal evolution of multiple bodies in terrestrial orbit (*Canup et al.*, 1999) suggests that the two moon states will destabilize (through either mutual collision or collision of one of the moons with the Earth), and that an inner massive moon will likely sweep up smaller outer debris as it tidally evolves outward.

While simulations of both lunar accretion and the long-term evolution of bodies in Earth orbit appear to naturally predict an end state of a single moon, forming a lunar-mass moon remains problematic. Comparisons between predictions of impact simulations and results of the lunar accretion simulations are currently underway. However, to date a single impact has yet to be identified that can simultaneously account for the masses of the Earth and the Moon, as well as the current system angular momentum (*Cameron and Canup*, 1998; *Canup et al.*, 2000; see also chapter by *Cameron*, 2000). The only impacts thus far simulated that produce sufficient amounts of ejecta involve either impacts with angular momenta of about twice that of the Earth-Moon system, or an impact with a reduced-mass Earth that is only about 70% accreted after the moon-forming impact (see chapter by *Cameron*, 2000).

In this chapter, we review the accretion models, which describe the evolution of a particulate protolunar disk composed of a distribution of solid bodies. We note that this likely may not correspond well to the earliest state of the protolunar disk (a state that the impact simulations do not yet unambiguously constrain), or to the physical state of the disk material as it collisionally evolves. Below we first outline basic timescale arguments for the postimpact evolution of the disk; for additional discussion, see *Thompson and Stevenson* (1988), and reviews by *Stevenson* (1987) and *Pritchard and Stevenson* (2000).

Timescales for cooling from a lunar mass, optically thick protolunar disk radiating as a blackbody are $\sim 10\text{--}100$ yr. By far the fastest process in the disk is collisions between ejected bodies, with the characteristic time between collisions given by $t_{\text{col}} \sim 1/(\tau\Omega) \sim 4 \times 10^3 (a/3 R_{\oplus})^{3/2} (1/\tau)$ s, where τ is optical depth and $\Omega \equiv (GM_{\oplus}/a^3)^{1/2}$ is the orbital frequency at a semimajor axis a . For $\tau \sim 1$ at $a = 3 R_{\oplus}$, t_{col} is about 1 hr. Collisions damp relative energies, causing the disk to flatten, and exchange angular momentum, causing the disk to spread. The timescale for disk spreading is $t_{\text{spread}} \sim a^2/\nu$, where ν is viscosity; t_{spread} is much longer than the collision time in most disks. The standard kinematic viscosity is a function of the velocity dispersion v and t_{col} : $\nu \sim v^2 t_{\text{col}}$. For a $2 M_{\oplus}$ uniform surface density disk composed of mass m particles extending to $a \sim 3 R_{\oplus}$, $t_{\text{spread}} \sim 6 \times 10^{20}/m$ yr, where m is in grams and we have assumed $v \sim v_{\text{esc}}$, where v_{esc} is the surface escape velocity of the disk particles. However, disk-spreading times can be much shorter than this estimate for a massive disk subject to gravitational instability (*WC77*). Instability-induced clumps are not stable within the Roche limit, but lead to enhanced collision rates that in turn yield a much larger effective viscosity, $\nu_{\text{eff}} \propto G^2 \Sigma^2 / \Omega^3$ where Σ is the disk surface density (*WC77*; see also *Lin and Pringle*, 1987). This is the same functional form

for viscosity that was later found by *KIM00* using a somewhat different physical argument (see section 3, equation (31)). N-body simulations of the protolunar disk have confirmed the rapid timescale for disk spreading predicted by *Ward and Cameron*, with $t_{\text{spread}} \sim$ months. However, such rapid rates may be physically unrealistic when the thermal and radiative properties of the disk are taken into account. *Thompson and Stevenson* (1988) recognized that the rate of spreading in the protolunar disk may be fundamentally regulated by the ability of the disk to radiate the gravitational binding energy liberated as the disk spreads. In this case, t_{spread} is on the order of the disk cooling time, or $10\text{--}100$ yr, vastly longer than that predicted using the viscosity derived in *WC77*.

When material in the disk has cooled and solidified, mutual collisions will result in fragmentation for high impact velocities, and in accretion if relative velocities are $\leq v_{\text{esc}}$. However, in a massive protolunar disk, the rate of collision may be so high as to remelt or even revaporize disk material during the accretion process (see discussion in chapter by *Pritchard and Stevenson*, 2000). Once massive bodies are present, they will experience orbital evolution due to tidal interaction with both the disk and the Earth. Using the current terrestrial tidal dissipation factor, the orbital evolution time for a lunar mass body with $a = 3 R_{\oplus}$ due to terrestrial tides is on the order of years to decades, longer than nominal accretion times implied by N-body simulations.

It thus should be recognized that the protolunar disk may evolve significantly prior to the point at which its state could be aptly described by a particulate distribution of solid bodies, which is the assumption inherent to all the simulations described in this chapter. Indeed, the nature of the protolunar disk viscosity and its associated spreading time will be functions of the initial thermal state of the ejected material, as well as the subsequent evolution of the disk's energy budget as it spreads and accretes. To date, models have not included such processes, and it is thus unclear whether current simulations offer an adequate description of the disk viscosity and temporal evolution. This is particularly true in the inner disk, where material is most likely to have been significantly heated. The need for further investigation of these issues has been highlighted by a new theory for the origin of the Moon's orbital inclination (*Ward and Canup*, 2000). This theory relies on a resonant interaction between the newly formed Moon and an inner remnant disk, the effectiveness of which is dependent upon the viscosity, lifetime, and mass of the inner disk.

However, the main finding of the accretion simulations to date — a relationship between the mass of the moon and the initial angular momentum of the disk — should be relatively independent of the exact physical nature of the disk material. Assuming that the disk angular momentum is provided by the original impact event, the final size of the moon that can accrete just outside the Roche limit is constrained by a simple conservation of angular momentum argument, regardless of the mode of angular momentum transport in the disk.

In this chapter, we describe the general results of the accretion simulations, which are relatively insensitive to choice of initial disk conditions over the parameter space explored to date. In section 2, we outline a parameterization for modeling the tidal inhibition of accretion near the Roche limit. Section 3 describes the results of N-body simulations of the protolunar disk, and section 4 discusses the long-term evolution and stability of material in terrestrial orbit. Section 5 offers a summary and discusses areas for future research.

2. MODELING ACCRETION NEAR THE ROCHE LIMIT

Traditionally, simulations of accretion in a circumsolar protoplanetary disk (e.g., *Greenberg et al.*, 1978; *Nakagawa et al.*, 1983; *Spaute et al.*, 1991; *Wetherill and Stewart*, 1993; *Weidenschilling et al.*, 1997) have utilized two-body approximations to describe interactions between orbiting bodies. For example, a standard accretion criterion is that the rebound velocity following a collision must be less than the two-body escape velocity of the colliding pair. Such approaches are valid if the physical size of an orbiting object is much smaller than its Hill sphere, as is the case for orbits well outside the classical Roche limit. For an impact-generated disk, $\langle a \rangle \sim a_R$, and a three-body treatment is required to account for tidal inhibition of accretion near and within the Roche limit. In this section, we review developments in tidal accretion models, focusing on the model utilized in lunar accretion simulations.

2.1. The Hill Three-Body Formalism

The Hill approximation describes the motion of two bodies orbiting a much more massive central body using a rotating coordinate system. The Hill coordinate system is defined so that the x axis points radially outward, the y axis is tangent to a circular orbit, and the z axis is normal to the orbital plane. The angular velocity of the coordinate system is just the Keplerian orbital frequency, $\Omega = (GM_c/a_0^3)^{1/2}$, where a_0 is the reference orbital radius and M_c is the mass of the central body. For a complete derivation, see *Nakazawa and Ida* (1988).

Hill's equations are often written in nondimensionalized form, with time scaled by Ω^{-1} and length scaled by the product (ha_0) , where h is the reduced Hill radius. For a pair of orbiting bodies with masses m_1 and m_2 , $h \equiv [(m_1 + m_2)/(3M_c)]^{1/3}$. The linearized equations of relative motion in nondimensionalized Hill units are

$$\begin{aligned} \ddot{x} &= 2\dot{y} + 3x - \frac{3x}{r^3} \\ \ddot{y} &= -2\dot{x} - \frac{3y}{r^3} \\ \ddot{z} &= -z - \frac{3z}{r^3} \end{aligned} \quad (1)$$

where x , y , and z are the relative coordinates in the rotat-

ing frame and $r = (x^2 + y^2 + z^2)^{1/2}$. The $(2\dot{y})$ and $(-2\dot{x})$ terms represent Coriolis forces, and those proportional to $1/r^3$ are the mutual gravity terms. The tidal terms are $(3x)$ and $(-z)$: The tidal acceleration is positive in the radial direction (acting to increase the separation of the orbiting bodies), negative in the vertical direction (acting to decrease the relative separation of the orbiting bodies), and has no component in the azimuthal direction.

A constant of the motion described by equation (1) is the Jacobi energy

$$E_J = \frac{1}{2}(\dot{x}^2 + \dot{y}^2 + \dot{z}^2) + U(x, y, z) \quad (2)$$

where $U(x, y, z)$ is the Hill potential

$$U(x, y, z) = -\frac{3}{2}x^2 + \frac{1}{2}z^2 - \frac{3}{r} + \frac{9}{2} \quad (3)$$

The first two terms of U are the tidal potential, and the third is the mutual gravity between the orbiting objects. The constant $9/2$ has been added so that U vanishes at $(x, y, z) = (\pm 1, 0, 0)$, i.e., the L_1 and L_2 Lagrangian points. Figure 1 shows the Hill potential in the $z = 0$ plane. The $U = 0$ surface defines the Hill “sphere,” which is actually lemon-shaped with a half-width (in Hill units) of unity in the radial direction, $2/3$ in the azimuthal direction, and ≈ 0.64 in the vertical direction. The Hill sphere is roughly the region of space within which the gravity of an orbiting object dominates the motion of nearby particles.

For orbits near the Roche limit, the physical size of an orbiting body becomes comparable to the size of its Hill sphere. The Hill radius of an isolated orbiting body of mass

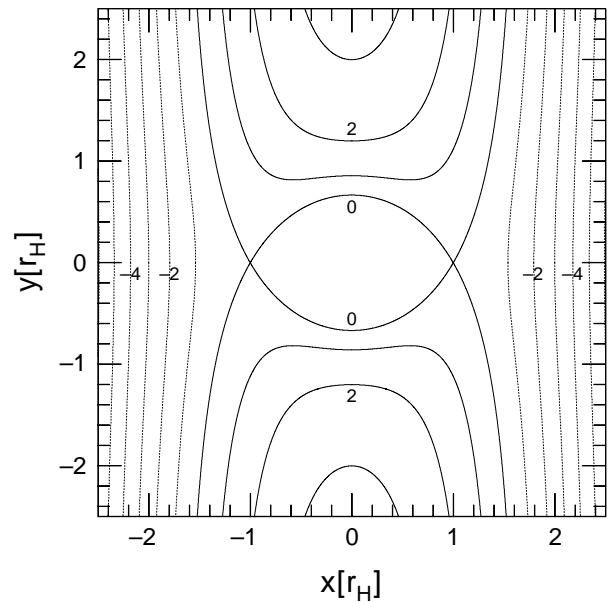


Fig. 1. The Hill potential for the $z = 0$ plane; units are in Hill units (time scaled by Ω^{-1} and length scaled by $r_H = ha_0$).

m is just $r_H = [m/(3M_c)]^{1/3}a$. The ratio between the physical radius of a body and its Hill radius is

$$\frac{r}{r_H} = 3^{1/3} \left(\frac{\rho}{\rho_c} \right)^{-1/3} \frac{R_c}{a} \quad (4)$$

where R_c and ρ_c are the radius and density of the central body, and ρ is the density of the orbiting body. This ratio can also be expressed in terms of the classical Roche limit for a fluid, strengthless body

$$\frac{r}{r_H} \approx 0.6 \left(\frac{a_R}{a} \right) \quad (5)$$

where

$$a_R \equiv 2.456 \left(\frac{\rho}{\rho_c} \right)^{-1/3} R_c \quad (6)$$

For $a \gg a_R$ (and so $r \ll r_H$), encounters between objects are well described by two-body approximations that ignore the gravity of the central body. However, if $a \sim a_R$ (or if relative velocities are comparable or less than the quantity $ha_0\Omega$, known as the Hill velocity), a three-body approach is required to describe interactions and collisional outcomes.

2.2. Tidal Accretion Criteria

Early models for accretion near the Roche limit were developed to describe collisions in planetary rings. *Weiden-schilling et al.* (1984) incorporated tidal effects into their ring evolution model by allowing for disruption of bodies when a size-dependent tidal stress exceeded an assumed internal strength. However, it was later argued (*Longaretti*, 1989) that gravity must be the dominant mechanism for accretion of bodies larger than a few centimeters. *Longaretti* (1989) derived a tidal accretion condition by determining the equilibrium between the tidal force and the mutual gravitational force between a pair of orbiting particles aligned radially with respect to the central planet. This defined a critical mass ratio for a pair of colliding bodies below which gravitational accretion could occur, which was equivalent to the requirement that the sum of the radii of the colliding bodies must be less than (ha_0) for accretion. Henceforth we will refer to the quantity (ha_0) as the mutual Hill radius.

A somewhat different set of conditions results if a tidal model is developed using an energy rather than a force approach. *Ohtsuki* (1993) observed that since the Hill potential $U = 0$ surface is closed, two objects cannot escape their mutual Hill sphere if their postcollision relative energy, E'_J , is negative. From this $E'_J < 0$ condition, *Ohtsuki* derived a maximum coefficient of restitution that would allow for accretion assuming $r \ll r_H$ and neglecting the tidal terms in equation (3). For the case of $r \sim r_H$, *Ohtsuki* (1993) performed numerical integrations of collisions, concluding that the probability for accretion dropped rapidly for $r \geq 0.7 r_H$. *Canup and Esposito* (1995, hereafter *CE95*) expanded on

Ohtsuki's approach, including the tidal terms in U and deriving capture criteria for the $r \sim r_H$ and $a \sim a_R$ case. These criteria include (1) a critical mass ratio for accretion [of the same form as that found by *Longaretti* (1989) but somewhat more restrictive] and (2) a critical coefficient of restitution. These constraints define a ‘‘Roche zone’’: the region surrounding the classical Roche limit where tidally modified accretion occurs (*CE95*). Below we review the derivation of these basic tidal accretion criteria, which can be easily incorporated into statistical or direct integration accretion simulations.

As two bodies collide, E_J is just

$$E_J = \frac{1}{2} v_{\text{imp}}^2 - \frac{3}{2} x_p^2 + \frac{1}{2} z_p^2 - \frac{3}{r_p} + \frac{9}{2} \quad (7)$$

where v_{imp} is the scaled impact velocity, and x_p , y_p , and z_p are the coordinates of the impact point, such that $x_p^2 + y_p^2 + z_p^2 = r_p^2$. Here r_p is

$$r_p \equiv \frac{r_1 + r_2}{ha_0} \quad (8)$$

which can also be expressed as

$$r_p = \frac{R_c}{a_0} \left(\frac{\rho}{3\rho_c} \right)^{-1/3} \frac{1 + \mu^{1/3}}{(1 + \mu)^{1/3}} \approx 0.6 \left(\frac{a_R}{a_0} \right) \frac{1 + \mu^{1/3}}{(1 + \mu)^{1/3}} \quad (9)$$

where μ is the mass ratio of the colliding objects, with $0 < \mu \leq 1$. The postcollision energy is (*Ohtsuki*, 1993)

$$E'_J = \frac{1}{2} \varepsilon^2 v_{\text{imp}}^2 - \frac{3}{2} x_p^2 + \frac{1}{2} z_p^2 - \frac{3}{r_p} + \frac{9}{2} \quad (10)$$

Here ε is an effective coefficient of restitution given by

$$\varepsilon = \left(\frac{\varepsilon_n^2 v_n^2 + \varepsilon_t^2 v_t^2}{v_n^2 + v_t^2} \right)^{1/2} \quad (11)$$

where the v_n and v_t are the normal and tangential components of the relative impact velocity and ε_n and ε_t are the normal and tangential coefficients of restitution. When the velocity and orientation of an impact are both known (e.g., in an N-body simulation), the $E'_J < 0$ test for accretion for a given collision can utilize equation (10) directly. Below we derive accretion criteria averaged over all impact orientations.

If two bodies collide with random orientation, averaging equation (10) over all impact orientations gives the angle-averaged rebound energy (*CE95*)

$$E'_J = \frac{1}{2} \varepsilon^2 v_{\text{imp}}^2 - \frac{3}{r_p} - \frac{1}{3} r_p^2 + \frac{9}{2} \quad (12)$$

The specific choice of impact orientation affects the coefficient of the r_p^2 term; here we have assumed random impact

orientation. The r_p^2 coefficient is $3/2$ in the case of impacts occurring in the radial direction, $-1/2$ for impacts in the vertical direction, and 0 for impacts oriented in an azimuthal direction. The above equation can also be written as

$$E_J' = \frac{1}{2} (\varepsilon^2 v_{\text{imp}}^2 - v_{\text{esc,3B}}^2) \quad (13)$$

where $v_{\text{esc,3B}}$ is an angle-averaged three-body escape velocity (CE95)

$$v_{\text{esc,3B}} \equiv \sqrt{6/r_p + 2r_p^2/3 - 9} \quad (14)$$

The scaled two-body escape velocity is just $\sqrt{6/r_p}$.

A necessary condition for $E_J' < 0$ is that the term $v_{\text{esc,3B}}^2$ is positive, because the term $\varepsilon^2 v_{\text{imp}}^2$ is always positive. This condition requires that

$$r_p \leq 0.691 \quad (15)$$

Note that $v_{\text{esc,3B}}^2$ is also positive for $r_p > 3.3$, but in this case the bodies are well outside their Hill sphere and cannot remain gravitationally bound. The physical meaning of equation (15) is that $(r_1 + r_2)$ must be less than the angle-averaged Hill radius. For E_J' to be negative, $v_{\text{esc,3B}}^2$ must also be larger than $\varepsilon^2 v_{\text{imp}}^2$. The latter condition yields a critical coefficient of restitution

$$\varepsilon < \varepsilon_{\text{cr,3B}} \equiv \frac{v_{\text{esc,3B}}}{v_{\text{imp}}} \quad (16)$$

Thus when the physical size of colliding bodies exceeds about 70% of their mutual Hill radius they will not on average remain gravitationally bound, even if collisions are completely inelastic. This differs from the two-body approximation, in which completely inelastic collisions always result in accretion. Equation (15) is also a more stringent requirement than that obtained by Longaretti (1989) using a force approach to model escape in the radial direction, which yields an $r_p < 1$ criterion. This is because escape from the Hill sphere is also possible azimuthally and vertically, and the Hill “sphere” is actually narrower in these directions.

Equations (9) and (15) define a critical mass ratio for accretion for a completely inelastic ($\varepsilon = 0$) collision as a function of orbital location and particle density (CE95)

$$\frac{(1 + \mu_{\text{cr}})^{1/3}}{1 + \mu_{\text{cr}}^{1/3}} = \left(\frac{1}{0.691} \right)^{3^{1/3}} \frac{R_c}{a_0} \left(\frac{\rho}{\rho_c} \right)^{-1/3} \quad (17)$$

where μ_{cr} is the maximum mass ratio that two bodies can have in order to remain gravitationally bound after a completely inelastic collision. Figure 2 is a plot of the critical mass ratio for accretion as a function of orbital radius, with the classical Roche limit shown for comparison. The critical accretion curve in Fig. 2 was derived assuming random impact orientation; a choice of a specific impact orientation (e.g., a radial impact) shifts the curves along the x-axis but does not change their form (see, e.g., Fig. 4). Note that the

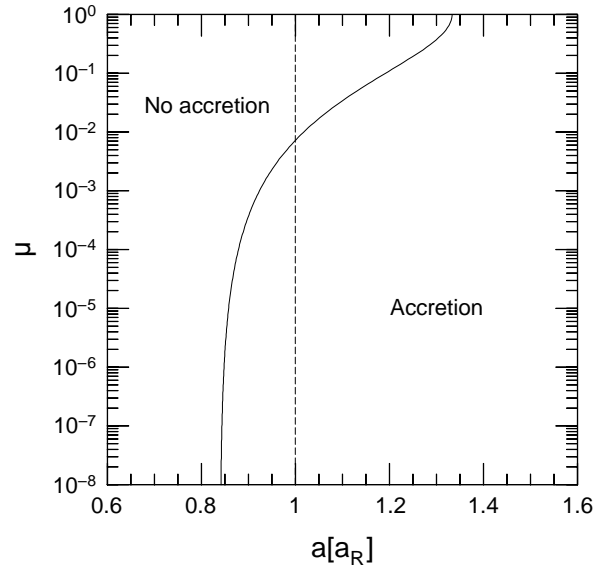


Fig. 2. The angle-averaged critical mass ratio for accretion as a function of scaled orbital radius and particle density for completely inelastic collisions ($\varepsilon = 0$). Here a_R is the classical Roche limit (dashed line), which is a function of the ratio of particle to planetary density (see text for details). Accretion is precluded by tidal forces on average for impacts occurring with random impact orientation to the left of the mass ratio curve.

accretion of like-sized ($\mu = 1$) bodies is tidally inhibited within a region that extends beyond the classical Roche limit, while pairs with low mass ratios can accrete interior to a_R .

2.3. Character of Tidal Accretion

The three-body accretion criteria discussed above define three basic regimes of accretional growth surrounding the Roche radius. For orbits interior to about $0.85 a_R$, bodies overflow the mean width of their Hill sphere and tidal effects on average preclude accretion. Accretion in the range of $0.85 a_R \leq a \leq 1.4 a_R$ (defined by CE95 to be the “Roche zone”) is mass ratio dependent: collisions between bodies with a mass ratio less than μ_{cr} may result in accretion if rebound energies are low enough. Bodies with mass ratios larger than μ_{cr} cannot on average remain gravitationally bound, even for completely inelastic collisions. For orbits exterior to about $1.4 a_R$, accretion is possible between objects of all sizes.

The parameterizations of tidal effects discussed here are simplistic, and represent only a first-order approach to the problem. Potentially important physical effects have yet to be included, or really even investigated. For example, implicit in the derivation has been the assumption that colliding bodies are spherical and will bounce in a manner similar to billiard balls, rebounding in an intact state with a given coefficient of restitution. The outcome of a collision near the Roche limit might be quite different if the collision energy

were high enough to fragment a significant amount of the mass of one or both of the colliding bodies. In this case, the pulverized fragments might more easily be able to avoid physically protruding from the Hill sphere. Another assumption involves the use of the standard Hill approximation to describe the local potential of two bodies in contact that are similar in size with $r_p \sim 1$. In this case, the distribution of mass is far from spherically symmetric, and would likely cause a distortion of the local potential and the shape of the Hill “sphere” from the standard Hill approximation. Orbiting bodies would also likely be rotating before and after collisions, the effects of which were not included in *Ohtsuki* (1993) or *CE95*.

Finally, the criteria described here have been derived using a three-body approach, and any local clumping of material in the region of a collision could collectively influence collisional outcomes in a manner different than that predicted here. For example, local simulations of collisional evolution within Saturn’s rings suggest that the formation of gravitational wakes fosters the buildup of temporary aggregates (*Salo, 1992*; see also discussion in *CE95*); such clumping is also observed in the lunar accretion simulations. However, direct N-body integrations that treat all collisions as inelastic rebounds and explicitly model mutual interactions show the growth of aggregates in a similar manner as that predicted by the tidal accretion criteria reviewed above (see section 3).

The tidal accretion criteria do a credible job of accounting for the gross characteristics of the planetary ring systems around the outer planets (e.g., *Longaretti, 1989*; *CE95*; *Canup and Esposito, 1997*). The location of the Roche zone, the variation of the inhibition of accretion with orbital radius, and the mass-ratio dependence of tidal accretion appear to coincide qualitatively well with a fundamental observed transition in all the outer satellite systems — from inner rings, to coexisting rings and moons, to outer isolated moons. This basic agreement is important, as the current ring and inner satellite systems are a direct observable relevant to a dynamical state through which the protolunar disk may have evolved.

3. N-BODY SIMULATION OF LUNAR ACCRETION

In this section, we focus on lunar accretion as modeled using direct N-body orbital integrations. In the evolution of a protolunar disk, global effects such as radial migration of lunar material, interaction of formed moons with the disk, and collective effects such as the formation of particle aggregates are potentially important. The merit of N-body simulation is that all gravitational interactions are explicitly accounted for, while the main disadvantage of this technique is its high computational cost. *ICS97* were the first to use N-body simulation to investigate the evolution of a protolunar disk and lunar formation. Inspired by the work of *ICS97*, *KIM00* performed higher-resolution N-body simulations of a protolunar disk and investigated the evolution of the spatial structure of the disk in detail. The main

result of the simulations by both *ICS97* and *KIM00* is that, in most cases, a single large moon is formed just outside the Roche limit on a timescale of a month, with a nearly circular orbit close to the equatorial plane of the initial disk. The mass of the moon is linearly dependent on the initial disk angular momentum.

In this section, we focus on three points: (1) why a single moon is the typical outcome of the disk evolution, (2) what determines the timescale of lunar accretion from a protolunar disk, and (3) the relation between the mass of the accreted moon and the initial disk condition.

3.1. Method of Calculation

3.1.1. Orbital integration. In an N-body simulation, the orbits of particles are calculated by numerically integrating the equation of motion

$$\frac{d\mathbf{v}_i}{dt} = -GM_\oplus \frac{\mathbf{x}_i}{|\mathbf{x}_i|^3} - \sum_{j \neq i}^N Gm_j \frac{\mathbf{x}_i - \mathbf{x}_j}{|\mathbf{x}_i - \mathbf{x}_j|^3} \quad (18)$$

where m , \mathbf{x} , and \mathbf{v} are the mass, position, and velocity of disk particles respectively, and G is the gravitational constant. The first term of the righthand side of equation (18) represents the Earth’s gravity, and the second is the mutual gravitational interaction of disk particles. *ICS97* and *KIM00* did not include the force due to tidal bulges raised on the Earth by orbiting bodies, since the timescale of orbital evolution due to terrestrial tides is much longer than the accretional timescale (*CE96*). The J_2 component of Earth’s gravity ($\approx 10^{-3}$ at present; $\approx 10^{-2}$ at the time of formation) was also not included. For numerical integration, both *ICS97* and *KIM00* used the predictor-corrector type Hermite scheme (*Makino and Aarseth, 1992*; *Kokubo et al., 1998*).

The most expensive part of N-body simulation is the calculation of the mutual gravitational force, whose cost increases in proportion to the square of the number of particles. However, the recent development of software and hardware for N-body simulation has made it possible to consider more than 10^4 particles in a protolunar disk simulation, compared to the 10^3 particles utilized in *ICS97*. In the *KIM00* simulations, mutual gravitational forces were calculated by directly summing up interactions of all pairs of particles on the special-purpose computer, HARP-3/GRAPE-4 (*Makino et al., 1993, 1997, Makino and Taiji, 1998*).

3.1.2. Collision and accretion. Collisions between particles play an important role in the evolution of a protolunar disk. In an N-body simulation, a collision occurs when the distance between two particles equals the sum of their radii. It is assumed that two colliding particles rebound with a relative rebound velocity \mathbf{v}' , which is determined by the relative impact velocity \mathbf{v} and the coefficients of restitution

$$\begin{aligned} \mathbf{v}'_n &= -\epsilon_n \mathbf{v}_n \\ \mathbf{v}'_t &= \epsilon_t \mathbf{v}_t \end{aligned} \quad (19)$$

The velocity of each particle after the collision is then calculated based on conservation of momentum. *KIM00* and

ICS97 performed simulations with two values for the normal coefficient of restitution, $\epsilon_n = 0.1$ and 0.01 ; the tangential component was fixed at $\epsilon_t = 1$ for simplicity. For these values, the effective coefficient of restitution given by equation (11) is $\epsilon \approx 0.7$.

In N-body accretion simulations, the initial particles in the disk are assumed to have infinite strength, so that they remain intact even at arbitrarily close distances to the Earth. This prevents the total number of bodies in a simulation from rapidly growing to a computationally unmanageable quantity. However, this assumption means that the simulated size distribution of material interior to the Roche limit likely contains bodies that are larger than those that in reality could have accreted there; for example, in the high-resolution simulations of *KIM00*, the smallest initial particles have $m \sim 10^{-5} M_\oplus$, or a diameter of about 60 km.

Given an initial distribution of disk particles, conditions for when collisions will result in accretion must be then specified. The necessary and sufficient conditions for gravitational binding between two orbiting particles are that (1) the Jacobi energy of the two bodies (equation (10)) after the collision is negative, and (2) the centers of mass of both colliding bodies are within their mutual Hill sphere. Because the Hill potential is nonaxisymmetric, both conditions depend on the angle of impact, as discussed in section 2. The *ICS97* simulations used the angle-averaged *CE95* accretion criteria, assuming that any collision with $E_J < 0$ and $(r_1 + r_2) < 0.7 r_H$ resulted in a merger. The merged spherical body was assigned a total mass equal to that of the colliding bodies, and its position and velocity were set equal to those of the center of mass of the collision. In a merging event, some fraction of the orbital angular momentum of two colliding bodies would in reality be transferred into the spin of the merged body. However, the spin angular momentum obtained by many merging events is generally much smaller than the orbital angular momentum, and so the total orbital angular momentum of a system during a simulation is very nearly conserved. Merged bodies were assumed to have infinite strength, so that a merged body that accreted outside the Roche limit remained intact even if it later strayed within a_R .

The *KIM00* simulations expanded on *ICS97* by considering three different formalisms for collisional outcomes. The first, called the “partial accretion model,” was identical to that utilized in *ICS97*. In the second model, the “total accretion model,” the condition for merger was relaxed so that accretion was assumed for collisions after which $E_J < 0$ and $(r_1 + r_2) < r_H$. In a final set of simulations, *KIM00* did not allow for any mergers, and instead simply allowed particles to bounce inelastically. In this “rubble pile model,” gravitationally bound aggregates of particles form outside the Roche limit, and are tidally disrupted when they stray too close to Earth. In both the rubble pile and sometimes in the partial accretion model, gravitationally bound particles can remain in contact with one another even though they are not formally merged.

While the total and partial accretion models both assume that mergers create bodies of infinite strength, the rubble

pile model assumes that merged aggregates have no strength and are held together only by their self-gravity. In the case of a strengthless, deformable fluid body, the classical Roche limit defines the minimum distance for an object to remain gravitationally bound, which from equation (5) implies $r \leq 0.6 r_H$ for stability. Physical reality would fall somewhere in between the infinite strength and strengthless approximations.

KIM00 found that the results of the total and partial accretion models and the rubble pile model are quantitatively similar over relatively short dynamical timescales. Over longer dynamical timescales, the rubble pile model differs slightly because, in this case, the moon loses some mass during collisions with other aggregates and through tidal stripping. The results of both the total and partial accretion models are essentially the same over long dynamical timescales.

3.1.3. Initial conditions. *ICS97* and *KIM00* started their simulations of lunar accretion assuming a solid particle disk. As the initial properties of an impact-generated disk are uncertain, and because the disk may significantly evolve before it cools and may be able to be treated as a particulate distribution, both *ICS97* and *KIM00* modeled the protolunar disk using a wide array of initial conditions. The initial mass distribution of disk particles was modeled by a power-law mass distribution

$$n(m)dm \propto m^{-\alpha}dm \quad (20)$$

where $n(m)$ is the number of particles of mass m . The density of disk particles is $\rho = 3.3 \text{ g cm}^{-3}$ (the bulk lunar density) and the density of the Earth is $\rho_\oplus = 5.5 \text{ g cm}^{-3}$. Disk particles are assumed to be spheres. The initial disk is axisymmetric, with a power-law surface density distribution given by

$$\Sigma(a)da \propto a^{-\beta}da \quad (21)$$

where a is the distance from the Earth, with inner and outer cutoffs, a_{in} and a_{out} . The assumption of disk axisymmetry should be valid because a nonaxisymmetric disk becomes axisymmetric due to Keplerian shear on a timescale of several Kepler times (approximately days). The initial eccentricities and inclinations of particles are assumed to be Rayleigh distributed. The ratio of the RMS eccentricity to the RMS inclination was fixed as $\langle e^2 \rangle^{1/2} / \langle i^2 \rangle^{1/2} = 2$. In general, the initial distributions of eccentricities and inclinations do not affect the disk evolution since they relax with a timescale on the order of the Kepler period due to collisional damping.

KIM00 studied the evolution of two initial disk masses, $2 M_\oplus$ and $4 M_\oplus$. They also varied the power index of the surface density distribution ($\beta = 1, 3, 5$) and the outer cutoff of the disk ($a_{\text{out}} = 0.5, 1, 1.5, 2 a_R$), which is equivalent to changing the initial specific angular momentum of the disk, j_{disk} . The j_{disk} values were varied over the range

$$0.62\sqrt{GM_\oplus a_R} \leq j_{\text{disk}} \leq 1.0\sqrt{GM_\oplus a_R}$$

The effects of the power index of the mass distribution and

the initial velocity dispersion on the result were also tested. The power-law exponent of the mass distribution was chosen to be $\alpha = 0.5, 1.5, 2.5, \infty$, with a dynamic range in mass of $m_{\max}/m_{\min} = 1000$ for the $\alpha \neq \infty$ cases ($\alpha = \infty$ corresponds to an equal-mass case).

3.2. Evolution of a Protolunar Disk

KIM00 performed 60 simulations with the total and partial accretion models, and 10^4 initial particles. They followed the evolution of the disk for $1000 T_K$, where T_K is the Kepler period at the distance of the Roche limit and $T_K \approx 7$ hr. The disk evolution is qualitatively similar for all the simulations in *KIM00* and *ICS97*, although the initial disk conditions, the accretion model utilized, and the number of initial disk particles were varied.

In Figs. 3–5, we show an example of the evolution of a 10^4 -particle disk as simulated by *KIM00*. The initial disk has a mass $M_{\text{disk}} = 4 M_\oplus$ with $\alpha = 1.5$, $\beta = 3$, $a_{\text{in}} = R_\oplus$, $a_{\text{out}} = a_R$, and $\langle e^2 \rangle^{1/2} = 0.3$. The coefficients of restitution were assumed to be $\epsilon_n = 0.1$ and $\epsilon_t = 1$ and the total accretion model was adopted.

Figure 3 shows snapshots of the protolunar disk in the R - z plane for $t = 0, 10, 20, 100, 1000 T_K$. The protolunar disk first flattens through collisional damping and then expands radially. A single large moon forms around $R \approx 1.4 a_R$ on a nearly noninclined circular orbit on a timescale of $\sim 100 T_K$. These are universal characteristics of the accreted moon in all the simulations by *KIM00* and most of the *ICS97* simulations, and appear to be nearly independent of initial disk conditions.

The orbital radius of the location of each merging collision and the mass ratio of the accreted particles are plotted in Fig. 4. The angle-averaged *CE95* critical mass-ratio is shown as well as the total accretion model condition, $r_p < r_H$. As the total accretion model was adopted here, accretion was possible to the right of the curve $r_p < r_H$. In $t = 0$ – $10 T_K$, disk particles spread outward and start to accrete with one another if the accretion conditions are satisfied. In the total accretion model, accretion becomes possible for $m_2/m_1 = 10^{-3}$ beyond $a \approx 0.65 a_R$. The minimum mass ratio of 10^{-3} at this stage reflects the initial mass dynamic range. The accretion location spreads outward as the disk expands, and accretion between particles with small mass difference occurs in $t = 10$ – $20 T_K$. The rapid formation of the moon occurs in $t = 20$ – $100 T_K$. In this stage, the formation of relatively large moonlets and collisions among them make a single large moon. The accretion between particles that differ greatly in mass around $R = 1.3 a_R$ indicates the accretion of disk particles by the growing moon. The moon gradually migrates outward due to interaction with the disk while still accreting some material in $t = 100$ – $1000 T_K$, although the growth rate is low.

The mass of the largest moon, M , and the mass fallen to the Earth, M_{fall} , are plotted vs. time in Fig. 5. The mass of material that escapes from the gravitational field of the Earth is usually smaller than 5% of the initial mass of the disk.

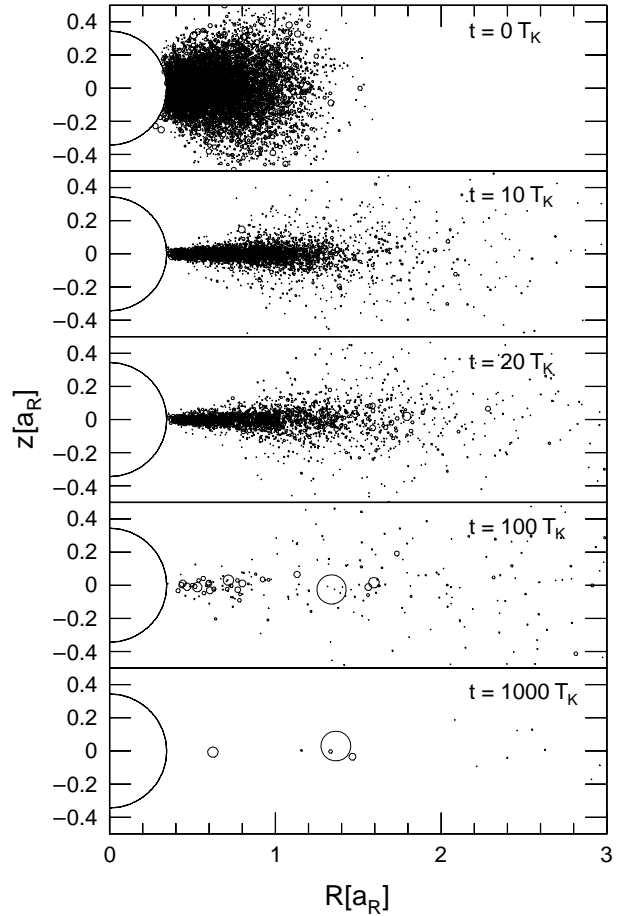


Fig. 3. Snapshots of the protolunar disk on the R - z plane at $t = 0, 10, 20, 100,$ and $1000 T_K$. The semicircle centered at the coordinate origin represents the Earth. Disk particles are shown as circles whose size is proportional to the physical size of disk particles.

The mass of the moon at $t = 1000 T_K$ is $0.85 M_\oplus$, while $3.1 M_\oplus$ of the initial disk mass has fallen to the Earth. The fraction of the disk mass incorporated into the moon varies with the initial disk conditions.

The evolution of the disk is divided into two stages, namely, the rapid growth and slow growth stages as seen in Figs. 3 and 5. The duration of the rapid growth stage is $\sim 100 T_K$, or about 1 month. In this stage, the redistribution of disk mass through angular momentum transfer supplies material for accretion outside the Roche limit: Most of the disk mass falls to the Earth while some of the mass is transported outward (see Fig. 5). The formation of the moon is almost completed in this stage. The slow growth stage after $\sim 100 T_K$ is the “cleaning up stage,” where the moon sweeps up and scatters away the residual disk mass.

3.2.1. Formation of a single moon. In order to see why a single large moon is a typical outcome of the disk evolution, we examine the rapid growth stage in detail. The evolution of the spatial structure of the disk in the rapid growth

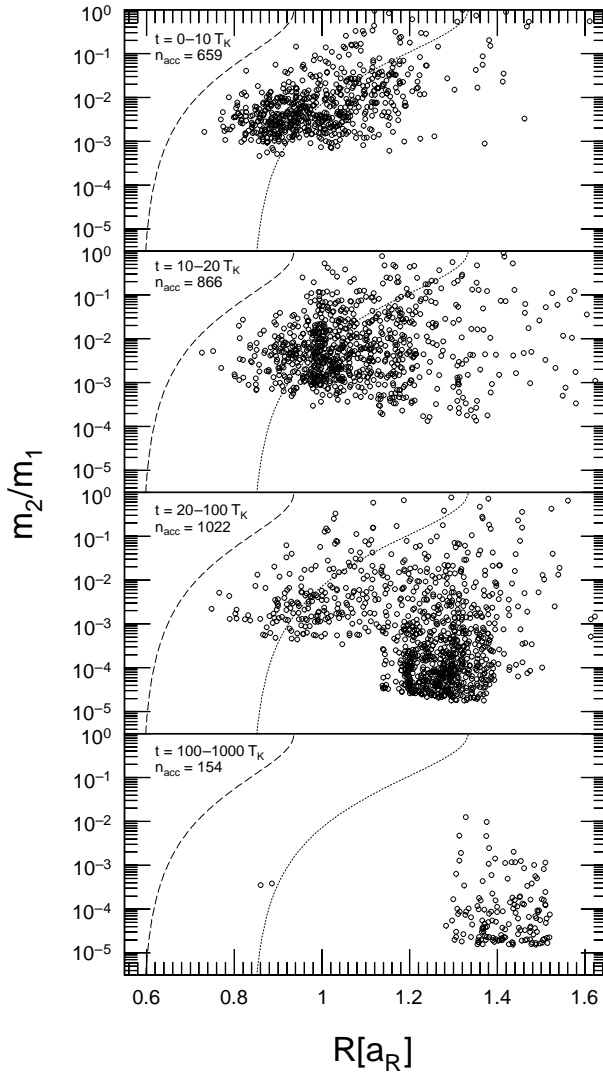


Fig. 4. The mass ratio m_2/m_1 of two accreted particles vs. the orbital radius of the location of the accreting event for the time periods $t = 0-10$, $10-20$, $20-100$, and $100-1000 T_K$. The total number accreting events in each period is n_{acc} . The angle-averaged tidal accretion condition (dotted curve) and the total accretion model condition $r_p \leq r_H$ (dashed curve) are also shown.

stage is most easily seen by the rubble pile model, since in this model gravitationally bound particles are not merged but form particle aggregates. Snapshots of the disk in the x - y plane are shown for $t = 0, 1, 5, 10, 20$, and $40 T_K$ in Fig. 6. The initial condition of the disk here is the same as that shown above except here an equal-mass initial distribution was considered. Figure 7 shows snapshots of the radial profile of the surface density. The surface density drops to zero at the surface of the Earth ($R_{\oplus} = 0.34 a_R$). At $t = 40 T_K$ of Fig. 6, a large bound aggregate with a mass of about one-half the present Moon is formed at $R \approx 1.3 a_R$, which is consistent with the result of the total and partial accretion models.

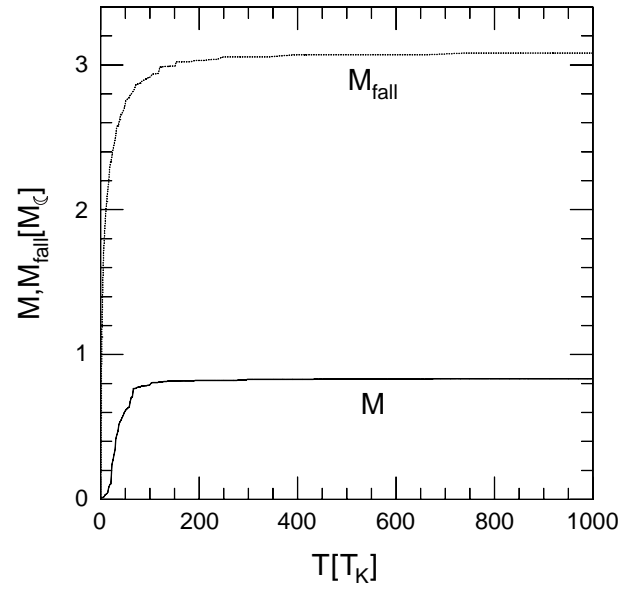


Fig. 5. The moon mass M (solid curve) and the mass fallen to the Earth M_{fall} (dotted curve) as a function of time.

Before examining the disk evolution in further detail, we briefly discuss the stability of a differentially rotating disk. Disk stability has been studied extensively in the context of galactic and circumstellar disks (see, e.g., *Binney and Tremaine, 1987*). In a disk, self-gravity tends to produce density contrasts, while the random motion of constituent particles and the tidal force (shear) smooth it. It is convenient to introduce Toomre's Q parameter (*Toomre, 1964*)

$$Q \equiv \frac{v_R \Omega}{\pi G \Sigma} \quad (22)$$

where v_R is the radial velocity dispersion of disk particles and Ω is the angular velocity of the disk. When $Q > 1$, that is, when the effect of the tidal force or the random motion overwhelms that of the self-gravity of the disk, the disk is gravitationally stable and density contrasts do not grow in the disk. In fact, a particulate protolunar disk is marginally stable, but instability still plays an important role in the disk evolution. In terms of a_R , Q is given by

$$Q \sim 0.1 \left(\frac{\rho_{\text{disk}}}{\rho} \right)^{-1} \left(\frac{a}{a_R} \right)^{-3} \quad (23)$$

where ρ_{disk} is the spatial density of disk material and ρ is the internal density of the disk particles (*Ida et al., 2000*).

The evolution of an initially compact disk in the rapid growth stage is described below:

1. Contraction of the disk. The initial disk is dynamically “hot” (high relative velocities) and Toomre's Q value is much larger than unity ($t = 0 T_K$ of Fig. 6), so that the

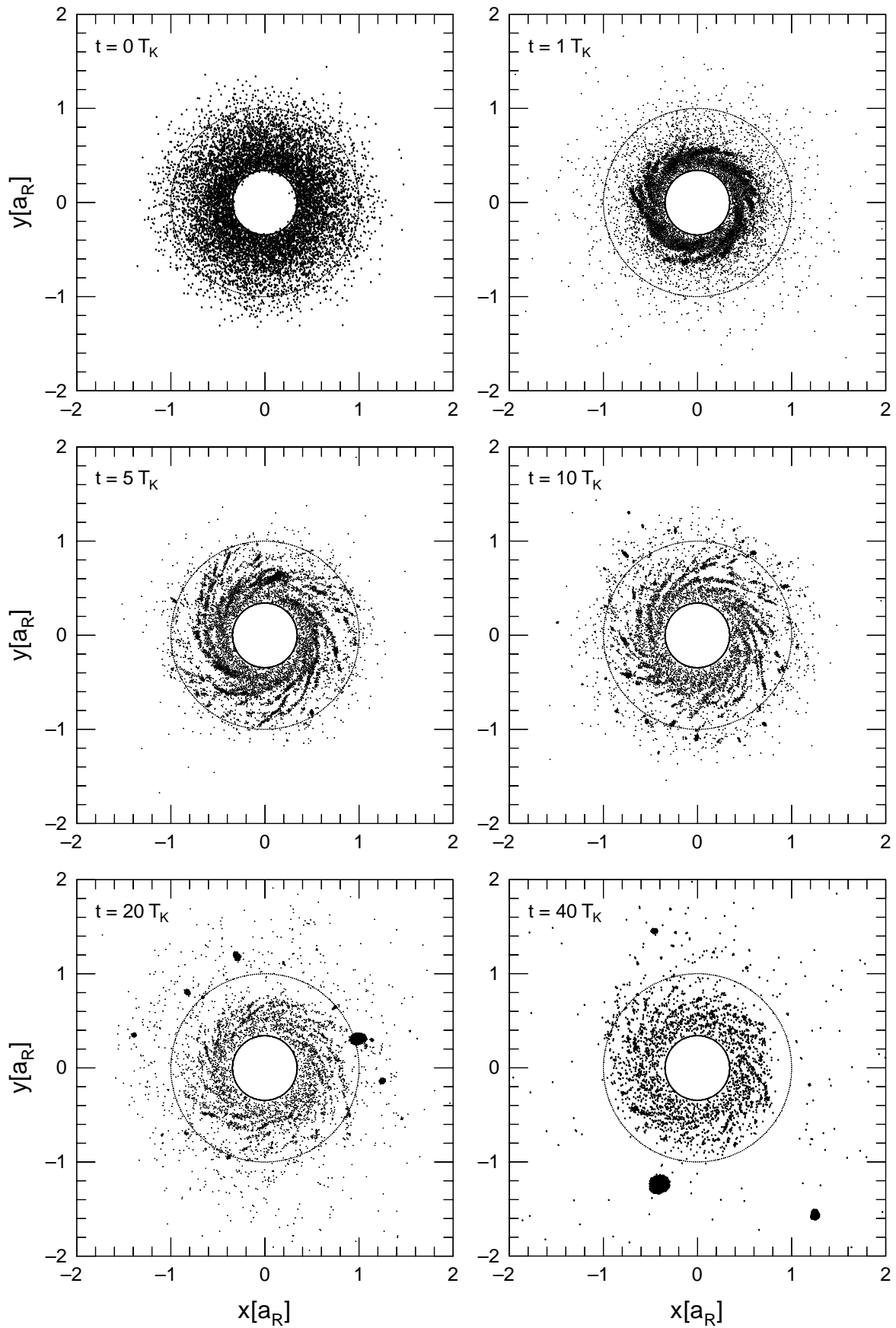


Fig. 6. Snapshots of the circumterrestrial disk on the x - y plane at $t = 0, 1, 5, 10, 20,$ and $40 T_K$.

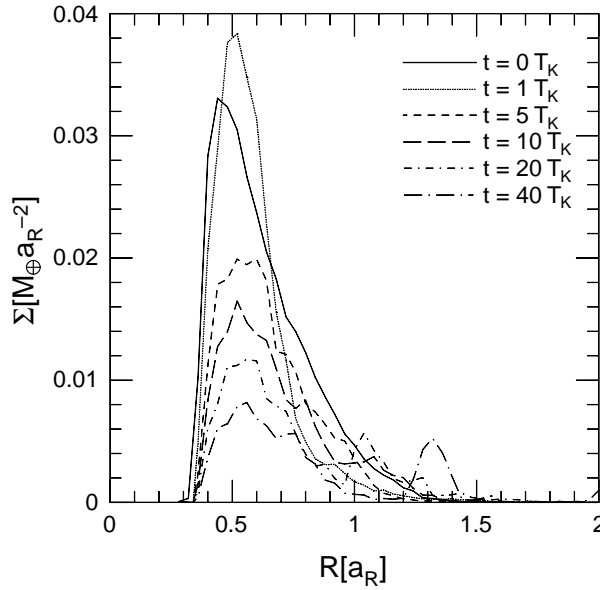


Fig. 7. The surface density Σ is plotted as a function of the distance from the Earth R for $t = 0, 1, 5, 10, 20,$ and $40 T_K$.

disk is gravitationally stable. First the disk shrinks radially and vertically because the velocity dispersion decreases through collisional damping. The timescale of this contraction is of the order of T_K since the initial optical depth of the particulate disk in the simulation is of order of unity and the coefficient of restitution for particles is less than unity.

2. Formation of clumps. As the velocity dispersion decreases, Q decreases. At this time particle clumps grow near $a \approx 0.5 a_R$ where Q has its minimum value $Q \sim 1$ ($t = 1 T_K$).

3. Formation of spiral arms. The clumps are soon destroyed by the tidal force because they are within the Roche limit. They become elongated due to Keplerian shear, which results in the formation of spiral arm-like structures ($t = 5 T_K$). The radial wavelength of the spirals, as well as the size of the clumps, is roughly consistent with the critical wavelength with $Q = 1$ expected from linear stability analysis (e.g., Toomre, 1964)

$$\lambda \sim \lambda_c \equiv \frac{2\pi^2 G \Sigma}{\Omega^2} \sim 2\pi a \frac{M_{\text{disk}}}{M_{\oplus}} \quad (24)$$

For $a = 0.5 a_R$ and $\Sigma = 0.03 M_{\oplus} a_R^{-2}$, $\lambda_c \sim 0.1 a_R$, which is consistent with the results in Fig. 6. Since the pitch angle of the spiral arms is moderate, the number of spiral arms is estimated by

$$n_s \approx \frac{2\pi a}{\lambda_c} \sim \frac{M_{\oplus}}{M_{\text{disk}}} \quad (25)$$

For $M_{\text{disk}} = 4 M_{\oplus}$, $n_s \sim 20$, which is consistent with results of N-body simulations. The spiral arms are transient material waves, not pattern waves, and are not gravitationally

bound inside the Roche limit. The spiral arms are sheared out as they wind up, and then the cycle is repeated, as gravitational instability leads to the formation of clumps that are elongated to form spiral arms again.

4. Mass transfer by spiral arms. Particles are transferred outside the Roche limit through the gravitational torque exerted by the spiral arms, in compensation for the inward evolution of many particles to Earth. The surface density inside the Roche limit decreases with time due to mass transfer to Earth and beyond the Roche limit. On the other hand, since the simulated disk was initially entirely within the Roche limit, the surface density outside a_R increases with time as material spreads outward. While the mass (and angular momentum) is effectively transferred by spiral waves, Q is kept around 2 (e.g., Salo, 1995; Daisaka and Ida, 1999).

5. Collapse of aggregates. When a tip of a spiral arm extends beyond the Roche limit, it collapses into a small aggregate ($t = 10 T_K$). Outside the Roche limit, particles in contact in the aggregate are gravitationally bound. The mass of the aggregate is approximately given by

$$m \approx \pi \Sigma \left(\frac{\lambda_c}{2} \right)^2 \sim \pi^2 \left(\frac{M_{\text{disk}}}{M_{\oplus}} \right)^2 M_{\text{disk}} \quad (26)$$

The formation of aggregates outside the Roche limit in the rubble pile model corresponds to the formation of moonlets in the accretion models.

6. Formation of a lunar seed. By sweeping up the small aggregates, a large aggregate quickly grows on a timescale of $10 T_K$ ($t = 20 T_K$). A single large aggregate (the lunar seed) is formed at $a \approx 1.1 a_R$, with a nearly noninclined and circular orbit.

7. Growth of the lunar seed. The lunar seed stays just outside the Roche limit and continues to sweep up particles spreading beyond the Roche limit. As the lunar seed grows, it moves gradually outward due to interaction with the inner disk. The peak of the surface density at $t = 40 T_K$ ($R \approx 1.3 a_R$) corresponds to the lunar seed.

As a massive and compact particulate disk evolves in the manner described above, a single large moon forms inevitably. The relations (24), (25), and (26) also hold in simulations with somewhat different values of M_{disk} . Note that if the initial disk is radially extended past the Roche limit, accretion is immediately possible in the outer disk, which may result in a temporary multiple moon system (Canup et al., 1999).

3.2.2. Timescale of lunar accretion. *KIM00* showed that the timescale of the rapid growth stage is of the order of $100 T_K$ (approximately 1 month), relatively independent of the initial conditions they simulated. Assuming that the initial disk is contained primarily within the Roche limit, the moon forms from material spreading beyond a_R , so that the predicted timescale of lunar formation is almost equivalent to the timescale of the mass and angular momentum transfer due to the gravitational torque by the spiral arms. The angular momentum flux through a right circular cylinder

centered on the disk axis is given by

$$F_g = \frac{1}{4\pi G} \int_0^{2\pi} R d\theta \int_{-\infty}^{\infty} dz \frac{\partial \Phi}{\partial R} \frac{\partial \Phi}{\partial \theta} \quad (27)$$

where Φ is the disk potential (*Lynden-Bell and Kalnajs, 1972*). For a disk with a spiral pattern whose potential can be represented by

$$\Phi_s(R, \theta) = -\frac{2\pi G}{|k|} \Sigma_s(R) e^{i[n_s\theta + f(R)]} \quad (28)$$

where k is a radial wavenumber of the spiral pattern in the tight-winding approximation, $\Sigma_s(R)$ gives the amplitude of the spiral pattern, and $f(R)$ is the shape function of the spiral pattern (see, e.g., *Binney and Tremaine, 1987*), the angular momentum flux is given by (*Lynden-Bell and Kalnajs, 1972*)

$$F_g = \frac{\pi^2 n_s G R \Sigma_s^2}{k^2} \quad (29)$$

Substituting the critical wavenumber $k_c = 2\pi/\lambda_c = \Omega^2/(\pi G \Sigma)$ for k and Σ for Σ_s and using $n_s = kR \tan i$, we obtain

$$F_g = \frac{\pi^3 G^2 R^2 \Sigma^3 \tan i}{\Omega^2} \quad (30)$$

where i is the pitch angle of the spiral arms. The effective viscosity for the angular momentum flux due to the gravitational torque exerted by the spiral arms, defined as $\nu_g = F_g/(3\pi R^2 \Sigma \Omega)$ (*Lynden-Bell and Pringle, 1974*), is thus

$$\nu_g = \frac{\pi^2 \tan i}{3} \frac{G^2 \Sigma^2}{\Omega^3} \quad (31)$$

Using this effective viscosity, the timescale of the angular momentum transfer by the spiral arms is estimated as

$$T_g \equiv \frac{(\Delta R)^2}{\nu_g} \sim 10^2 \left(\frac{\Sigma}{0.01 M_\oplus a_R^{-2}} \right)^{-2} \left(\frac{\Delta R}{0.5 a_R} \right)^2 \left(\frac{a}{a_R} \right)^{-9/2} T_K \quad (32)$$

where ΔR is the radial shift of material due to angular momentum transfer and we have used $\tan i \approx 1$. This timescale agrees well with the results of the N-body simulations by *KIM00* and *ICS97*. The functional form of T_g shows that the timescale of angular momentum transfer, in other words, the timescale of lunar accretion, depends on not the individual mass of disk particles but rather on the surface density of the disk. *WC77* obtained almost the same viscosity and timescale by considering the energy dissipation in the clumps formed by gravitational instability.

The spiral structure is not always clear in the disk since it is often destroyed by gravitational scattering by large moonlets inside the Roche limit. However, the mass trans-

fer rate hardly changes. This is because for the mass transfer, the important point is not an exact spiral structure but a nonaxisymmetric structure. Detailed investigation of the angular momentum transfer in a particulate protolunar disk (T. Takeda, personal communication) shows that the gravitational torque exerted by the spiral arms is the dominant driver for angular momentum transfer near the Roche limit as long as the initial number of disk particles is larger than a few thousand for the disks modeled here.

For a compact disk (i.e., one initially within the Roche limit), the results of the rubble pile model show that the lunar seed is formed not by gradual pairwise collision of disk particles but collective particle processes: formation of clumps by gravitational instability, angular momentum transfer due to the gravitational torque due to the spiral arm-like structures, and collapse and collision of particle aggregates. The size of the clumps and the spiral arms are in this case determined by the critical wavelength λ_c of the disk, which is a function of the surface density. Mass transfer is driven by the gravitational torque by the spiral arms, whose time-scale depends on the surface density. Overall, the N-body simulations show that it is the surface density of the disk, rather than the properties of the individual particles, that governs the evolution of the disk. However, these interpretations are dependent on the assumption that the protolunar disk can be adequately modeled with 10^3 – 10^4 particles and that the thermal evolution of the disk material can be neglected.

3.2.3. Dynamical characteristics of the moon. In this section, we consider the relationship between the dynamical characteristics of the accreted moon and the initial protolunar disk that was investigated by both *ICS97* and *KIM00*. However, the results that a single large moon is formed at $R \approx 1.3 a_R$ and that a linear relationship exists between the mass of the moon and the initial disk angular momentum are essentially the same in all the simulations.

The orbital elements of the moon for all of the *KIM00* simulations are shown in Fig. 8. The semimajor axis of the moon in all cases is between a_R and $1.7 a_R$, determined mainly by the formation location of the lunar seed and the subsequent interaction with the disk. The lunar seed forms just outside the Roche limit and it is pushed outward from its birthplace somewhat by recoil from the inner disk (shepherding). The eccentricity and inclination of the moon are small due to dynamical friction and collisional damping; in most cases, they are < 0.1 . These values are almost independent of the detailed initial conditions of the disk, and are similar to the results in *ICS97*. The resultant semimajor axis of the moon is small compared with the present lunar semimajor axis. On a longer timescale, the moon migrates outward by the tidal interaction with the Earth, presumably sweeping up outer residual mass (see section 4). Material inside the co-rotation radius ($\approx 2.3 R_\oplus$ for an initial 5-hr terrestrial day) will tidally evolve inward and fall to the Earth.

In the majority of cases, the largest moon that accretes is much more massive than any other remaining body. However, in about one-third of the *ICS97* simulations a “two-moon” system was formed, defined to be one in which the

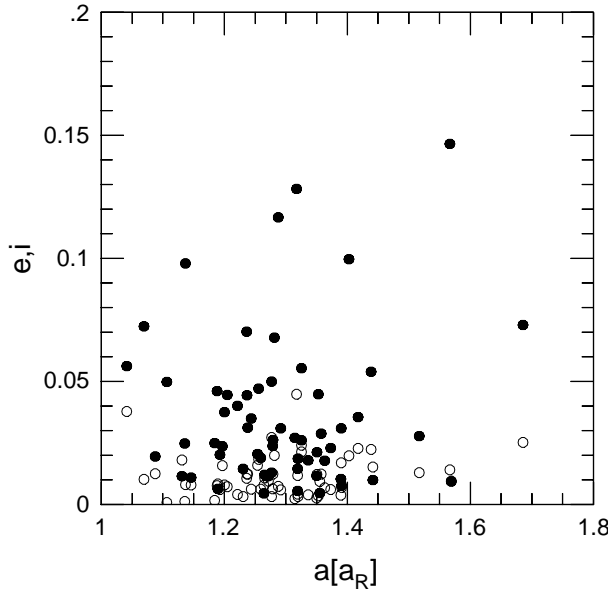


Fig. 8. The eccentricity (filled circles) and inclination (open circles) of the moon is plotted vs. the semimajor axis of the moon for all the runs.

mass of the second largest body exceeded 20% of the mass of the largest moon. In the *ICS97* two-moon cases, many of the second largest moonlets had orbital radii within the Roche limit, as they had been scattered inward subsequent to their formation. When estimating the number of two-moon systems formed from their simulations, *KIM00* ignored any moonlets inside a_R , assuming that in reality such bodies would be tidally disrupted. Given this assumption, *KIM00* found that only about 10% of their simulations yielded two-moon systems, and that in most of these cases the second largest moon was on a horseshoe orbit (i.e., in a 1:1 resonance) with the largest moon. A horseshoe moonlet is the survivor of the rapid moon formation stage when moonlets are formed and collide with one another. As collisions in this stage are stochastic, a moonlet can sometimes survive by being on a horseshoe orbit with the most massive moonlet.

In Fig. 9, the mass of the accreted moon, M , scaled by the initial disk mass is plotted vs. the initial specific angular momentum of the disk, j_{disk} , for all the *KIM00* simulations. For cases in which the moon had a companion on a horseshoe orbit, the sum of the moon and the horseshoe companion is plotted.

The results of *KIM00* and *ICS97* (their Fig. 5) show that M/M_{disk} increases linearly with j_{disk} . This is because in a small j_{disk} disk, (i.e., in a more compact disk), a greater amount of mass must fall to the Earth in order for some mass to spread beyond the Roche limit, yielding a smaller final moon. The fraction of material escaping from the Earth also increases with j_{disk} , although this fraction is usually less than 5% of the disk mass. The overall yield of incorporation of disk material into a moon(s) ranges from 10% to 55%.

ICS97 explained the relationship between the moon mass M and the specific angular momentum of the protolunar disk, j_{disk} , by using a conservation of mass and angular momentum argument. From conservation of mass, we have

$$M_{\text{disk}} = M + M_{\text{fall}} + M_{\text{esc}} \quad (33)$$

where M_{esc} is the total mass of material that escapes. Conservation of angular momentum gives

$$M_{\text{disk}} j_{\text{disk}} = M j + M_{\text{fall}} j_{\text{fall}} + M_{\text{esc}} j_{\text{esc}} \quad (34)$$

where j , j_{fall} , and j_{esc} are the mean specific angular momenta of the final moon, the mass that impacts the Earth, and the escaping mass, respectively, which are given by

$$j = \sqrt{GM_{\oplus}(1 - e^2)a}$$

$$j_{\text{fall}} = \sqrt{GM_{\oplus}(1 + e_{\text{fall}})q_{\text{fall}}}$$

$$j_{\text{esc}} = \sqrt{GM_{\oplus}(1 + e_{\text{esc}})q_{\text{esc}}}$$

where a , e , q_{fall} , e_{fall} , q_{esc} , and e_{esc} are the mean semimajor

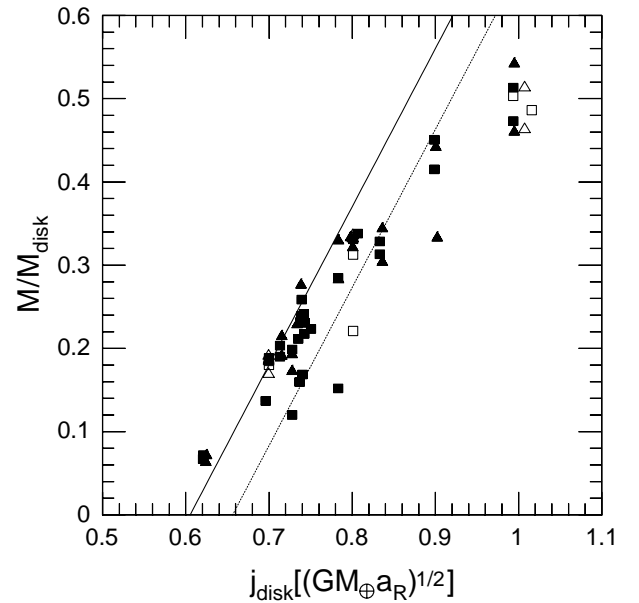


Fig. 9. The fraction of the initial disk mass incorporated into the moon, M/M_{disk} , is plotted against the initial specific angular momentum of the disk, j_{disk} , for all the *KIM00* runs. The triangles correspond to runs with an initial disk mass of $M_{\text{disk}} = 2 M_{\oplus}$ and the squares to runs with $M_{\text{disk}} = 4 M_{\oplus}$. The filled triangles and squares are for those runs assuming a coefficient of restitution $\epsilon_n = 0.1$, and the open ones for those assuming $\epsilon_n = 0.01$. The circles indicate runs that ended with two moons, defined to be those where the second largest moonlet has more than 20% of the mass of the largest moon. In these cases, the second-largest moon is on a horseshoe orbit with the largest moon, and the sum of the mass of the moon and the horseshoe orbiter is plotted. The theoretical estimate is also shown for $M_{\text{esc}} = 0$ (solid line) and $M_{\text{esc}} = 0.05 M_{\text{disk}}$ (dotted line).

axis and eccentricity of the moon, and the mean perigee distance and eccentricity of the Earth impactors and the escaping material respectively. This conservation argument assumes that the accretion disk is flat ($\langle i^2 \rangle^{1/2} \approx 0$) and that all material left in Earth orbit has been accreted into a single moon.

From equations (33) and (34), we obtain

$$M = \frac{(\dot{j}_{\text{disk}} - \dot{j}_{\text{fall}})M_{\text{disk}} + (\dot{j}_{\text{fall}} - \dot{j}_{\text{esc}})M_{\text{esc}}}{j - \dot{j}_{\text{fall}}} \quad (35)$$

The mean values of each orbital element obtained by *KIM00* are $\bar{a} = 1.3 a_R$, $\bar{e} = 0.04$, $\bar{q}_{\text{fall}} = 0.3 a_R \approx R_e$, $\bar{e}_{\text{fall}} = 0.2$, $\bar{q}_{\text{esc}} = 1.3 a_R$, and $\bar{e}_{\text{esc}} = 1.1$. The relation $\bar{q}_{\text{esc}} \approx \bar{a}$ reflects the fact that mass is ejected mainly due to gravitational scattering by the moon. Substituting these mean values into equation (35) yields

$$\frac{M}{M_{\text{disk}}} \approx 1.9 \frac{\dot{j}_{\text{disk}}}{\sqrt{GM_{\oplus}a_R}} - 1.1 - 1.9 \frac{M_{\text{esc}}}{M_{\text{disk}}} \quad (36)$$

This estimate is also shown in Fig. 9. The results of the high-resolution N-body simulations (*KIM00*) agree somewhat better than those of *ICS97* with the above analytic estimate, as *KIM00* found a somewhat larger moon mass.

Since M_{esc} is always much smaller than M_{disk} , we can neglect the M_{esc} terms in equation (35). In this case M is a function of j , \dot{j}_{fall} , \dot{j}_{disk} , and M_{disk} . However, j and \dot{j}_{fall} are not free parameters but always have almost the same values since j is determined by the fact that the moon forms just outside the Roche limit and \dot{j}_{fall} by the fact that remaining particles collide with the Earth. Then, the distribution of the disk mass to the moon and the Earth impactors is determined by the conservation of angular momentum. As the mass of the escapers is small compared with the disk mass, we can predict the mass of the moon from equation (36) when the mass and the angular momentum of the disk are given. *KIM00* confirmed that equation (36) holds for disks with masses in the range of $M_{\text{disk}} = 0.2\text{--}8 M_{\oplus}$.

The results of the N-body simulation deviate a little from the analytical estimate at low (~ 0.6) and high (~ 1.0) \dot{j}_{disk} . At the low end, the mass of the moon predicted by the simulations is larger than the analytical estimate because the semimajor axis of these moons and the specific angular momentum of the escaping material are smaller in these cases than the mean values used in equation (35). As the moons in the low \dot{j}_{disk} cases tend to be smaller in general, they suffer less gravitational recoil from the disk and move outward by a smaller distance, yielding a smaller moon semimajor axis than the mean value. For the high \dot{j}_{disk} cases, the analytical estimate of the lunar mass is larger than that obtained by the N-body simulations. At the end of these simulations, there are still about 1000 particles exterior to the moon, so that accretion is not yet complete. In fact, the sum of the mass of the moon and the mass of the particles bound to the Earth exterior to the moon (which would likely be the final moon mass), is on average $\sim 15\%$ larger than the lunar

mass at $t = 1000 T_K$, and more consistent with the analytical estimate.

In summary, as a consequence of the evolution of a particulate protolunar disk, a single large moon on a nearly noninclined circular orbit is formed just outside the Roche limit. This result hardly depends on the initial condition of the particulate disk, as long as

$$0.62\sqrt{GM_{\oplus}a_R} \leq \dot{j}_{\text{disk}} \leq 1.0\sqrt{GM_{\oplus}a_R}$$

$M_{\text{disk}} = 0.2\text{--}8 M_{\oplus}$, and $\epsilon_n = 0.01\text{--}0.1$, which may include the plausible conditions for the impact-generated disk. The moon is always formed around $a \approx 1.3 a_R$. In this case the mass of the moon is predicted simply by conservation of angular momentum from the initial disk. The accretion yields (the fraction of disk material incorporated into the moon) range from 10% to 55%.

4. EVOLUTION OF CIRCUMTERRESTRIAL MATERIAL

Two-thirds of the *ICS97* simulations produced a single large moon together with smaller bodies in exterior orbits; one-third yielded systems with two large moons. The great majority of the *KIM00* simulations yield the former case, while 10% yield two moons. While most accretion is complete after about a year, the final sweepup of material will occur over a longer time. Any bodies that remain on stable, noncolliding orbits after the initial accretion phase eventually must either collide with the Earth or be swept up by the moon as it orbitally evolves outward due to tidal interaction with the Earth. To date it has been assumed that the accretional stage of growth can be accurately modeled without including the effects of tidal evolution, as in general the tidal timescales are much longer than accretion times.

In this section, we address the question of whether or not a single moon will result from the likely end configurations of accretion in an impact-generated protolunar disk. For a complete discussion, see *Canup et al.* (1999; hereafter *CLS99*). Here we describe the basic tidal evolution process, and then discuss circumstances whereby moonlets and debris could become captured in mean-motion resonances as they tidally evolve. Such resonances are common among the satellites of the gas giant planets, and help to stabilize multiple moon systems in those cases. However, a terrestrial satellite system differs from the outer satellite systems in several key respects that predispose the terrestrial system to a single moon state.

4.1. Tidal Evolution of Moonlets

Exterior to synchronous orbit (the distance at which the orbital frequency equals the angular rotation rate of the Earth, $\approx 2.3 R_{\oplus}$ for a 5-hr terrestrial day), tides raised on Earth by an orbiting satellite lead to a transfer of angular momentum from Earth's rotation to the satellite's orbit, causing an increase in the orbital radius of the satellite.

Conversely, satellites within a_{sync} lose angular momentum and evolve inward due to terrestrial tides. A simple model for the rate of evolution of orbital radius due to this process can be used to estimate when two moons that are initially orbitally separated will evolve into orbits that are close enough to be unstable (*Canup and Esposito, 1996*). Once mutual collisions are possible between objects with $a > a_R$, the material involved will likely eventually accrete into a single body. Here we consider the system evolution until this occurs (for a description of the later tidal evolution of the Moon, see chapter by *Touma, 2000*).

The rate of evolution of orbital radius due to terrestrial tides is approximately given by

$$\left. \frac{da}{dt} \right|_{\oplus} \approx 3 k_2 \sqrt{\frac{G}{M_{\oplus}}} R_{\oplus}^5 m a^{-11/2} \sin(2\delta) \quad (37)$$

where k_2 is the Earth's second order Love number, m and a are the mass and orbital radius of the orbiting body, and δ is the tidal lag angle (e.g., *Burns, 1986*). For a constant lag angle, equation (37) can be integrated to yield the orbital position as a function of time

$$a(t) = \left(\frac{13}{2} K m t + a_0^{13/2} \right)^{2/13} \quad (38)$$

where

$$K \equiv 3 k_2 \sin(2\delta) \frac{R_{\oplus}^{13/2}}{M_{\oplus}} \sqrt{\frac{GM_{\oplus}}{R_{\oplus}^3}} \quad (39)$$

For sufficiently large t , $a(t) \propto (mt)^{2/13}$, and so the most massive moonlet will have the largest a value.

Consider two moonlets 1 and 2 with masses m_1 and m_2 and semimajor axes a_1 and a_2 (with $a_1 < a_2$). The evolution of the ratio (a_1/a_2) as two moonlets tidally evolve is important, because mean-motion resonances (which each occur at some characteristic (a_1/a_2) value) affect the system stability. A mean-motion resonance occurs when the ratio of the orbital motions of the two bodies is nearly a ratio of integers, e.g., for the $(p+q):p$ resonance, $\Omega_1/\Omega_2 \approx (p+q)/p$ where p and q are integers, and q is the order of the resonance. When two moonlets evolve through a resonance, the outcome is dependent upon whether $d(a_1/a_2)/dt$ is positive (typically referred to as the "converging" case) or negative (the "diverging" case).

From equation (37)

$$\frac{d}{dt} \left(\frac{a_1}{a_2} \right) = \frac{K}{a_2^2} (m_1 a_2 a_1^{-11/2} - m_2 a_1 a_2^{-11/2}) \quad (40)$$

The ratio (a_1/a_2) asymptotes to $(m_1/m_2)^{2/13}$, the value at which $d(a_1/a_2)/dt = 0$, (see *Canup and Esposito, 1996*). As two moonlets evolve to this asymptotic value, equation (40) implies three possible evolution paths: (1) $m_1/m_2 > 1$: moonlet 1 overtakes moonlet 2; (2) $(a_1/a_2)^{13/2} < m_1/m_2 < 1$: moonlet 1 does not overtake moonlet 2 and (a_1/a_2) increases to the

asymptotic value since $d(a_1/a_2)/dt > 0$; (3) $m_1/m_2 < (a_1/a_2)^{13/2}$: moonlet 1 does not overtake moonlet 2 and (a_1/a_2) decreases to the asymptotic value since $d(a_1/a_2)/dt < 0$.

In both (1) and (2), capture into resonance is possible, while capture is precluded in case (3). Before discussing further the effects of mean-motion resonances in the next section, we need to comment briefly on the evolution of satellite eccentricities due to tidal interaction.

From *Kaula (1964)* and *Goldreich and Soter (1966)*, the rate of change of eccentricity is

$$\left. \frac{de}{dt} \right|_{\text{tot}} \approx \frac{19e}{8a} \left. \frac{da}{dt} \right|_{\oplus} \left[\text{sgn}(\sigma) - \frac{28}{19} A \right] \quad (41)$$

where the first and second terms are due to tides raised on Earth and the satellite, respectively, $da/dt|_{\oplus}$ is given in equation (37), $\sigma = (2\omega - 3\Omega)$, ω is the angular rotation rate of the Earth, and A is defined as

$$A = \frac{k_2^* \sin(2\delta^*)}{k_2 \sin(2\delta)} \left(\frac{m}{M_{\oplus}} \right)^{-2} \left(\frac{R^*}{R_{\oplus}} \right)^5 \quad (42)$$

the ratio of satellite-to-planet effects used in *Mignard (1980, 1981)*; see also *Kaula, 1964*; *Burns, 1986*, where the starred quantities are those of the satellite. The lag angle δ is related to the tidal dissipation factor, Q , by $Q \sim 1/\sin(2\delta)$. For the current Earth-Moon system, $(k_2/Q)_{\zeta} \approx 0.0011$, $(k_2/Q)_{\oplus} \approx 0.021$, and so $A \sim 0.5$ (*Burns, 1986*; *Dickey et al., 1994*); thus currently de/dt from equation (41) is positive. However, we know that Q_{\oplus} has varied over the Moon's history, as its current value implies that the Moon achieved its present position after only about 2 b.y. (see *Burns, 1986*). Given this uncertainty, a range of A values from 0 to 20 is plausible during the Moon's evolutionary history, the latter representing a case where only solid body tides contribute to terrestrial dissipation.

4.2. Mean-Motion Resonances between Moonlets

As moonlets orbitally evolve due to tides they will pass through mutual mean-motion resonances. The evolution of the system during passage through or capture into an isolated resonance can be described by means of the adiabatic theorem (see, e.g., *Dermott et al., 1988*). Capture into resonance is only possible for converging orbits with $d(a_1/a_2)/dt > 0$; for co-planar orbits with $d(a_1/a_2)/dt < 0$, passage through resonance results only in a jump in eccentricity and not permanent capture (see *Dermott et al., 1988*; *Peale, 1986*).

Figure 10 is a plot of the asymptotic (a_1/a_2) value $[= (m_1/m_2)^{2/13}]$ due to tidal evolution as a function of moonlet mass ratio; also shown are the locations of first- and second-order mean-motion resonances. Below the solid curve orbits are tidally converging ($d(a_1/a_2)/dt > 0$), and capture into resonance is possible, depending on factors such as moonlet eccentricity and the rate of orbital evolution. Also shown (dashed line) is the critical (a_1/a_2) ratio for two-body sta-

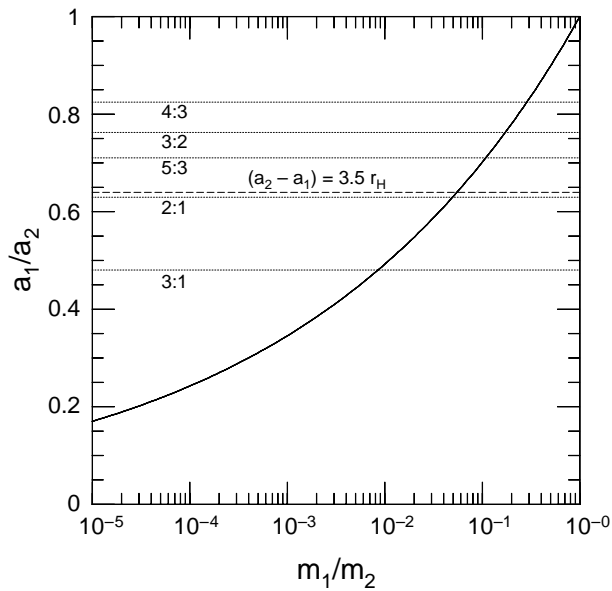


Fig. 10. The solid curve is the asymptotic value of (a_1/a_2) due to tidal interaction with the Earth as a function of moonlet mass ratio. Above and to the left of the curve, (a_1/a_2) decreases as moonlets tidally evolve; below and to the right, (a_1/a_2) increases due to tides. Also shown are the positions of first- and second-order mean-motion resonances (dotted lines). The dashed horizontal line is the (a_1/a_2) separation required for two-body stability with $(m_1 + m_2) = M_\oplus$. The only first- or second-order resonance that is well outside the $3.5 r_H$ stability separation in this case is the 3:1 (from *CLS99*).

bility [i.e., $(a_2 - a_1) \leq 3.5 r_H$] (*Gladman, 1993*) for $(m_1 + m_2) = M_\oplus$. Above this ratio, resonances are not isolated, orbits are chaotic, and mutual collisions can occur. Because of the large mass ratio of the Moon to the Earth, the only low-order resonance that lies well outside the two-body stability separation for bodies totaling a lunar mass is the 3:1. Thus there are a limited number of low-order resonances in which two Earth-orbiting moonlets whose total mass is a lunar mass could become captured.

CLS99 conducted a stability study for mean-motion eccentricity resonances in the protolunar disk using both analytical techniques and numerical simulations. In general, resonances lead to eccentricity growth, and so long-lived capture in a resonance requires that this growth is offset by eccentricity damping due to tidal evolution. From equation (41), it is seen that the effectiveness of the latter process is a function of A . For resonances where capture was possible, *CLS99* calculated equilibrium eccentricities due to the combined effects of the resonance and terrestrial and satellite tides, as a function of A . This approach, coupled with N -body integrations including the acceleration on orbiting bodies due to terrestrial tides, showed that the typical end states predicted by the *ICS97* simulations were unstable, and would likely yield a single moon in each case. Their findings are most easily summarized in terms of the initial relative positions and masses of the moonlets.

4.2.1. $m_1 > m_2$ case. In this case, orbits converge due to tides and it would appear likely that the inner moonlet would overtake and accrete the outer moonlet. However, capture into resonance can occur, which could prevent mutual collision. The equilibrium eccentricity for the outer body in an exterior mean-motion eccentricity resonance due to the combined effect of the resonance, and satellite and terrestrial tides is, in general, less than unity only for $A \geq 20$. Thus for $0 \leq A \leq 20$, exterior eccentricity resonances are unstable, and a massive inner moonlet will likely sweep up smaller outer moonlets as it tidally evolves outward.

4.2.2. $m_1 \sim m_2$ case. Here capture into resonance can occur, and stable equilibrium values of moonlet eccentricities in resonance are achieved for plausibly high rates of satellite dissipation (*CLS99*). However, in this case resonances destabilize as the relative importance of satellite to planetary tides approaches its current value of $A \sim 1$.

For the two-moon cases found in *ICS97* (which fall into this category), a more immediate issue for determining stability is the proximity of the inner moon to synchronous orbit, interior to which terrestrial tides lead to a decrease in orbital radius. *CLS99* found that the inner moon in all of the *ICS97* two-moon cases evolved inward and collided with the Earth in times as short as a year (assuming a terrestrial day of 5 hr).

4.2.3. $m_1 \ll m_2$ case. In this case, the asymptotic value of (a_1/a_2) achieved as bodies tidally evolve is smaller than that needed for instability [$(a_1/a_2) > 0.64$ for instability with two moonlets totaling a lunar mass]. The initial value of (a_1/a_2) would be greater than ~ 0.4 – 0.5 for potentially long-lived $m_1 \ll m_2$ pairs, assuming an outer moonlet with a ~ 1 – $1.5 a_R$ and an inner particle just outside the co-rotation radius ($2.3 R_\oplus$). In these cases, orbits tidally diverge [(a_1/a_2) decreases] and capture into resonance is precluded. The larger exterior body would tidally evolve outward and leave smaller inner bodies behind, potentially likely yielding a stable, multiple moon system. However, simulations do not predict that this configuration should persist after accretion from a protolunar disk, since perturbations by a moon that forms with close to a lunar mass appear to cause inner debris to collide with the Earth.

4.2.4. $a_1 \approx a_2$ case. Some recent accretion simulations predict the formation of moon pairs occupying horseshoe orbits (*KIM00*, see also section 3). The 1:1 resonance represents an interesting case, as tidal torques will cause the libration amplitude to decrease, increasing the stability of the resonance with time (e.g., *Yoder et al., 1983; Peale, 1986; Fleming and Hamilton, 2000*). Depending on the libration amplitude, the coorbital configuration could be destabilized through physical collisions with exterior objects encountered as the system tidally evolved outward. Another possibility is that scattering events with nearby objects could sufficiently increase eccentricities to allow for close encounters between the coorbitals.

Thus several factors appear to predispose a terrestrial system to a single moon state. First is the rapid rate of orbital evolution of satellites due to tidal interaction with the Earth.

Even for solid-body tidal Q values ($Q \sim 100$ s), a moon that forms close to the Earth evolves out to $20 R_{\oplus}$ (a typical outer limit for an impact-generated debris cloud; *Cameron and Benz, 1991*) in only 10^7 – 10^8 yr. Second, terrestrial Q values are within an order-of-magnitude of likely tidal Q values for orbiting satellites. This means that the plausible range of “ A values” — the relative role of satellite to planetary tides in affecting satellite eccentricity evolution extends only to $A \sim 20$, with a current value of $A \sim 0.5$ – 1 . For a satellite orbiting a gaseous planet, $A \sim 1000$, and satellite orbits are circularized by satellite tides. In a terrestrial system, planetary tides act to increase satellite eccentricities, destabilizing resonances and increasing mutual collisions. The large mass-ratio of the Moon to the Earth, coupled with lunar formation from a centrally condensed disk appears to insure that small inner disk material inside the Roche limit is effectively perturbed onto the Earth (*ICS97, KIM00*). However, an open question remains as to whether moonlet pairs that form in horseshoe orbits could remain stable over long times, and this issue merits investigation.

5. CONCLUSIONS

We have reviewed lunar accretion from a particulate protolunar disk that might result from a giant impact event. The typical radial extent of such a disk is believed to be on the order of the Roche limit, a_R . In the accretion process, terrestrial tidal forces and collective effects such as the development of spiral arms thus can play an important role in the protolunar disk case. The Earth’s tidal force partially inhibits accretion of particles in the Roche zone ($0.85 a_R \leq a \leq 1.4 a_R$), where accretion is dependent on the mass ratio of colliding bodies.

N-body integrations have been utilized to simulate the evolution of particulate protolunar disks, and have revealed that accretion in most such disks results in the formation of a single large moon. The moon is formed with $a \approx 1.3 a_R$ on a nearly noninclined, circular orbit. The evolution of a particulate protolunar disk consists of two basic stages. The first stage is a rapid growth stage, where material transferred outside the Roche limit as the disk spreads (together with material initially outside the Roche limit) self-gravitationally collapses and subsequently accretes to form a moon. The timescale for this stage is on the order of a month. Rapid angular momentum transfer by transient instabilities in the disk leads to the short (approximately 1 month) disk-spreading times, and orbital periods of only several hours yield a comparably short accretion time. These results hardly depend on the assumed initial condition of the disk, as long as the disk mass is on the order of $1 M_{\oplus}$ and it is assumed to be well represented by a particulate distribution. The second stage, in which the moon accretes material spreading outward from the inner disk, persists for about 1 yr. The moon masses predicted by the N-body simulations coincide well with analytical estimates based on conservation of angular momentum of the disk. The efficiency of incorporation of disk material into a moon is 10–55%, and the yield

increases linearly with the initial specific angular momentum of the disk. Recent simulations (with $N = 10,000$ particles) tend to predict a slightly larger moon mass and a higher probability of a single moon than previous simulations (with $N \sim 1000$). In cases of initial disks that radially extend beyond the Roche limit, multiple moons may result from the initial accretion phase. Simulations of the long-term evolution of multiple moons in terrestrial orbit, or of an inner moon with smaller exterior debris, find that all such systems destabilize as they tidally evolve, yielding a single moon in most cases.

The obtained (j_{disk} vs. M/M_{disk}) relationship tells us that in order to form a moon with a present lunar mass, we need

$$j_{\text{disk}} \approx 0.9 \sqrt{GM_{\oplus} a_R}$$

for $M_{\text{disk}} = 2 M_{\oplus}$ and

$$j_{\text{disk}} \approx 0.7 \sqrt{GM_{\oplus} a_R}$$

for $M_{\text{disk}} = 4 M_{\oplus}$ respectively. Thus, in order to form the present-sized moon from a light disk, the disk must be extended, while a compact disk may also yield a lunar-sized moon if it is very massive. This relationship thus provides an important constraint on the type of disk that must be created by a giant impact to yield the Moon. Simulations of the impact event to date suggest that to obtain the required disk we may need an impact with angular momentum significantly larger than the present Earth-Moon angular momentum, or an impact with a reduced-mass Earth (e.g., *Cameron and Canup, 1998; Canup et al., 2000*; see also chapters by *Cameron, 2000, and Canup and Agnor, 2000*).

An important factor that is not considered in previous, purely dynamical models is the thermal evolution of disk material. As a first step in investigating the evolution of a protolunar disk, the disk was assumed to be a particulate distribution. It is, however, believed that an entirely particulate distribution is not the most probable state for the protolunar disk when it condenses from the silicate vapor or liquid droplet cloud produced by the giant impact. Furthermore, the accretion timescale predicted by the N-body simulations is so short that it would be difficult for particles to cool by radiation in the course of accretion (e.g., *Thompson and Stevenson, 1988*). Indeed, a significant fraction of the accreted moon might be remelted or even reevaporated during accretion.

A coexistence of vapor/liquid and solid phases would be likely in the disk. Disk spreading and accretion might then instead proceed on the cooling timescale of the entire disk (~ 10 – 100 yr), much longer than the accretion time predicted by the N-body simulations of a particulate disk. However, a single large moon with mass predicted by equation (36) would likely still be the end result, as this is a basic consequence of conservation of angular momentum as we discuss below.

For example, consider lunar accretion from a disk composed of vapor, liquid, and solid phases. The outer disk would likely be cooler than the inner disk (due to a greater

surface area for radiative cooling and lower disk surface densities), so that the disk might consist of vapor/liquid components at small radii and of solid particles at large radii. As the outer particulate disk becomes dynamically cold through collisional damping, instabilities develop and rapidly transfer angular momentum in the outer disk. For this situation, we can estimate the mass of the accreted moon formed from only the outer particulate portion of the disk. Applying conservation of mass and angular momentum to the outer particulate disk, we can obtain a similar result as equation (36), where in this case we use the radius of the inner edge of the outer particulate disk for q_{fall} . Because the angular momentum transfer rate in the inner vapor/liquid disk would be significantly smaller than that in the outer particulate disk where spiral structure is prominent, it would be valid to consider mass and angular momentum transfer only within the outer disk. As the disk cools, the particulate region then extends inward. Finally when the disk becomes an entirely particulate disk, we may have the same relation as equation (36) as long as the accreted moon is located just outside of the Roche limit. This is because the lunar accretion is controlled by the mass and angular momentum conservations of the disk that are independent of the phase of lunar material. (If the inner vapor/liquid disk diffuses well beyond the Roche limit, moons might accrete well outside the Roche limit and the characteristics of the accreted moons might change.)

While the mass of the final moon may not be overly sensitive to thermal considerations, the specific properties of the Moon's orbit could be. Recently, *Ward and Canup* (2000) have shown that a single resonant interaction between a lunar-sized moon formed outside the Roche limit and an inner disk can increase the moon's orbital inclination from an initially low value (on the order of 1°) to values as high as 15° . This may offer a natural explanation for the origin of the Moon's initial inclination, which is known to have been $\sim 10^\circ$ from back integrations of the Moon's current orbit (see chapter by *Touma*, 2000). However, the *Ward and Canup* (2000) mechanism is effective only if an inner disk with at least 25% of a lunar mass persists for decades to centuries after the Moon accretes. Examination of these and other issues will require a new generation of protolunar disk models, including a detailed investigation of the evolution of a multiphase protolunar disk.

REFERENCES

- Benz W., Slattery W. L., and Cameron A. G. W. (1986) The origin of the moon and the single impact hypothesis I. *Icarus*, 66, 515–535.
- Benz W., Slattery W. L., and Cameron A. G. W. (1987) The origin of the moon and the single impact hypothesis II. *Icarus*, 71, 30–45.
- Benz W., Cameron A. G. W., and Melosh H. J. (1989) The origin of the moon and the single impact hypothesis III. *Icarus*, 81, 113–131.
- Binney J. and Tremaine S. (1987) *Galactic Dynamics*. Princeton Univ., Princeton.
- Burns J. A. (1986) The evolution of satellite orbits. In *Satellites* (J. A. Burns and M. S. Matthews, eds.), pp. 117–158. Univ. of Arizona, Tucson.
- Cameron A. G. W. (1997) The origin of the moon and the single impact hypothesis V. *Icarus*, 126, 126–137.
- Cameron A. G. W. (2000) Higher-resolution simulations of the giant impact. In *Origin of the Earth and Moon* (R. M. Canup and K. Righter, eds.), this volume. Univ. of Arizona, Tucson.
- Cameron A. G. W. and Benz W. (1991) The origin of the moon and the single impact hypothesis IV. *Icarus*, 92, 204–216.
- Cameron A. G. W. and Canup R. M. (1998) The giant impact occurred during Earth accretion (abstract). In *Lunar and Planetary Science XXIX*, Abstract #1062. Lunar and Planetary Institute, Houston (CD-ROM).
- Canup R. M. and Agnor C. B. (2000) Accretion of the terrestrial planets and the Earth-Moon system. In *Origin of the Earth and Moon* (R. M. Canup and K. Righter, eds.), this volume. Univ. of Arizona, Tucson.
- Canup R. M. and Esposito L. W. (1995) Accretion in the Roche zone: Co-existence of rings and ringmoons. *Icarus*, 113, 331–352.
- Canup R. M. and Esposito L. W. (1996) Accretion of the Moon from an impact-generated disk. *Icarus*, 119, 427–446.
- Canup R. M. and Esposito L. W. (1997) Evolution of the G-ring and the population of macroscopic ring particles. *Icarus*, 126, 28–41.
- Canup R. M., Levison H. F., and Stewart G. R. (1999) Evolution of a terrestrial multiple-moon system. *Astroph. J.*, 117, 603–620.
- Canup R. M., Ward W. R., and Cameron A. G. W. (2000) A scaling relationship for satellite-forming impacts. *Icarus*, submitted.
- Daisaka H. and Ida S. (1999) Spatial structure and coherent motion in dense planetary rings induced by self-gravitational instability. *Earth Planet Space*, 51, 1195–1213.
- Dermott S. F., Malhotra R., and Murray C. D. (1988) Dynamics of the uranian and saturnian satellite systems: A chaotic route to melting Miranda? *Icarus*, 76, 295–334.
- Dickey J. O., Bender P. L., Faller J. E., Newhall X X, Ricklefs R. L., Ries J. G., Shelus P. J., Veillet C., Whipple A. L., Wiant J. R., Williams J. G., and Yoder C. F. (1994) Lunar laser ranging: A continuing legacy of the Apollo program. *Science*, 265, 482–490.
- Fleming H. J. and Hamilton D. P. (2000) On the origin of the Trojan asteroids: Effects of Jupiter's mass accretion and radial migration. *Icarus*, submitted.
- Gladman B. (1993) Dynamics of systems of two close planets. *Icarus*, 106, 247–263.
- Goldreich P. and Soter S. (1966) Q in the solar system. *Icarus*, 5, 375–389.
- Greenberg R., Wacker J. F., Hartmann W. K., and Chapman C. R. (1978) Planetesimals to planets: Numerical simulation of collisional evolution. *Icarus*, 35, 1–26.
- Ida S., Canup R. M., and Stewart G. R. (1997) Lunar accretion from an impact-generated disk. *Nature*, 389, 353–357.
- Ida S., Kokubo E., and Takeda T. (2000) N-body simulations of moon accretion. In *Collisional Processes in the Solar System* (H. Rickman and M. Marov, eds.). Kluwer, in press.
- Kaula W. M. (1964) Tidal dissipation by solid friction and the resulting orbital evolution. *Rev. Geophys.*, 2, 661–685.
- Kipp M. E. and Melosh H. J. (1986) Short note: A preliminary numerical study of colliding planets. In *Origin of the Moon* (W. K. Hartmann, R. J. Phillips, and G. J. Taylor, eds.), pp. 643–

648. Lunar and Planetary Institute, Houston.
- Kipp M. E. and Melosh H. J. (1987) A numerical study of the giant impact origin of the Moon: The first half hour (abstract). In *Lunar and Planetary Science XVIII*, pp. 491–492. Lunar and Planetary Institute, Houston.
- Kokubo E., Yoshinaga K., and Makino J. (1998) On a time-symmetric Hermite integrator for planetary N-body simulation. *Mon. Not. R. Astron. Soc.*, 297, 1067–1072.
- Kokubo E., Makino J., and Ida S. (2000) Evolution of a circumterrestrial disk and formation of a single moon. *Icarus*, submitted.
- Lin D. N. C. and Pringle J. E. (1987) A viscosity prescription for a self-gravitating accretion disc. *Mon. Not. R. Astron. Soc.*, 255, 607–613.
- Longaretti P. (1989) Saturn's main ring particle size distribution: An analytic approach. *Icarus*, 81, 51–73.
- Lynden-Bell D. and Kalnajs A. J. (1972) On the generating mechanism of spiral structure. *Mon. Not. R. Astron. Soc.*, 157, 1–30.
- Lynden-Bell D. and Pringle J. E. (1974) The evolution of viscous discs and the origin of the nebular variable. *Mon. Not. R. Astron. Soc.*, 168, 603–637.
- Makino J. and Aarseth S. J. (1992) On a Hermite integrator with Ahmad-Cohen scheme for gravitational many-body problems. *Publ. Astron. Soc. Jpn.*, 44, 141–151.
- Makino J., and Taiji M. (1998) *Scientific Simulations with Special-Purpose Computers — The GRAPE Systems*. Wiley and Sons, Chichester.
- Makino J., Kokubo E., and Taiji M. (1993) HARP: A special-purpose computer for N-body problem. *Publ. Astron. Soc. Jpn.*, 45, 349–360.
- Makino J., Taiji M., Ebisuzaki T., and Sugimoto D. (1997) GRAPE-4: A massively-parallel special-purpose computer for collisional N-body simulations. *Astrophys. J.*, 480, 432–446.
- Mignard F. (1980) The evolution of the lunar orbit revisited, II. *Moon and Planets*, 23, 185–201.
- Mignard F. (1981) The lunar orbit revisited, III. *Moon and Planets*, 24, 189–207.
- Nakagawa Y., Hayashi C., and Nakazawa K. (1983) Accumulation of planetesimals in the solar nebula. *Icarus*, 54, 361–376.
- Nakazawa K. and Ida S. (1988) Hill's approximation in the three-body problem. *Prog. Theor. Physics Supp.*, 96, 167–174.
- Ohtsuki K. (1993) Capture probability of colliding planetesimals: Dynamical constraints on the accretion of planets, satellites and ring particles. *Icarus*, 106, 228–246.
- Peale S. J. (1986) Orbital resonances, unusual configurations and exotic rotation states among planetary satellites. In *Satellites* (J. A. Burns and M. S. Matthews, eds.), pp. 159–223. Univ. of Arizona, Tucson.
- Pritchard M. E. and Stevenson D. J. (2000) Thermal aspects of a lunar origin by giant impact. In *Origin of the Earth and Moon* (R. M. Canup and K. Righter, eds.), this volume. Univ. of Arizona, Tucson.
- Salo H. (1992) Gravitational wakes in Saturn's rings. *Nature*, 359, 619–621.
- Salo H. (1995) Simulations of dense planetary rings III. *Icarus*, 117, 287–312.
- Spaute D., Weidenschilling S. J., Davis D. R., and Marzari F. (1991) Accretional evolution of a planetesimal swarm: I. A new simulation. *Icarus*, 92, 147–164.
- Stevenson D. J. (1987) Origin of the Moon. *Annu. Rev. Earth Planet. Sci.*, 15, 271–315.
- Thompson C. and D. J. Stevenson (1988) Gravitational instability in two-phase disks and the origin of the Moon. *Astrophys. J.*, 333, 452–481.
- Toomre A. (1964) On the gravitational stability of a disk of stars. *Astrophys. J.*, 139, 1217–1238.
- Touma J. (2000) The phase space adventure of the Earth and Moon. In *Origin of the Earth and Moon* (R. M. Canup and K. Righter, eds.), this volume. Univ. of Arizona, Tucson.
- Ward W. R. and Cameron A. G. W. (1977) Disk evolution within the Roche limit (abstract). In *Lunar and Planetary Science IX*, pp. 1205–1207. Lunar and Planetary Institute, Houston.
- Ward W. R. and Canup R. M. (2000) Origin of the Moon's orbital inclination through resonant disk interactions. *Nature*, 403, 741–743.
- Weidenschilling S. J., Chapman C. R., Davis D. R., and Greenberg R. (1984) Ring particles: collisional interactions and physical nature. In *Planetary Rings* (R. Greenberg and A. Brahic, eds.), pp. 367–415. Univ. of Arizona, Tucson.
- Weidenschilling S. J., Spaute D., Davis D. R., Marzari F., and Ohtsuki K. (1997) Accretional evolution of a planetesimal swarm: 2. The terrestrial zone. *Icarus*, 128, 429–455.
- Wetherill G. W. and Stewart G. R. (1993) Formation of planetary embryos: Effects of fragmentation, low relative velocity, and independent variation of eccentricity and inclination. *Icarus*, 106, 190–209.
- Yoder C. F., Colombo G., Synnott S. P., and Yoder K. A. (1983) Theory of motion of Saturn's coorbiting satellites. *Icarus*, 53, 431–443.

